

MIGRATING MOTOR COMPLEX FORCE SENSOR: DESIGN, FABRICATION  
AND CLINICAL *IN VIVO* MEASUREMENTS

by

Matthew Michael Francisco

B.S., The Ohio State University, 2008

A thesis submitted to the  
Faculty of the Graduate School of the  
University of Colorado in partial fulfillment  
of the requirement for the degree of  
Master of Science  
Department of Mechanical Engineering

2013

This thesis entitled:  
Migrating Motor Complex Force Sensor: Design, Fabrication and Clinical *In vivo*  
Measurements  
written by Matthew Michael Francisco  
has been approved for the Department of Mechanical Engineering

---

Mark E. Rentschler, Ph.D.

---

Gregory B. Rieker, Ph.D.

Date \_\_\_\_\_

The final copy of this thesis has been examined by the signatories, and we find that both the content and the form meet acceptable presentation standards of scholarly work in the above mentioned discipline.

IRB protocol # 11-0157

Francisco, Matthew Michael (M.S., Department of Mechanical Engineering)

Migrating Motor Complex Force Sensor: Design, Fabrication and Clinical *In vivo*

Measurements

Thesis directed by Assistant Professor Mark E. Rentschler

In a continued effort to explore the human digestive tract for diagnostic and therapeutic purposes in a minimally invasive fashion, researchers are developing a new type of medical device: the robotic capsule endoscope (RCE). This small, untethered instrument is actively controlled by the physician and combines the functionality of traditional, flexible endoscopy with the versatility of a swallowable device. The narrow, convoluted geometry and active peristaltic forces within the small intestine represent the most challenging environment within the human gastrointestinal (GI) tract for a RCE to operate. A critical design parameter is the active peristaltic forces generated by the migrating motor complex (MMC) of the myenteron against a solid, non-deformable bolus.

In this work, a novel manometric sensor that measures the peristaltic forces generated by the MMC in a porcine model is modified for human use in a minimally invasive, sterile environment. Device modifications, calibration, and test methodology are presented. Results from multiple porcine and human *in vivo* tests of the sensor serve as a first-of-a-kind measurement that will benefit future RCE development.

# Acknowledgements

The author wishes to thank Dr. Jonathan Schoen for his time and surgical expertise involved with patient recruitment and *in vivo* testing of the device, Dr. Mark Rentschler for his guidance throughout the project, and Dr. Gregory Rieker for serving on his committee.

Additionally, the author wishes to acknowledge Dr. Benjamin Terry for his sensor design and testing, on which this work is based, Mr. Greg Potts for his generous time and expertise machining components for the sensor, and finally, the students of the Advanced Medical Technologies Lab for their help and support throughout this endeavor.

# Contents

Chapter 1: Introduction.....	1
1.1 Motivation.....	1
1.2 Scope .....	3
Chapter 2: Background.....	5
2.1 Gross Anatomy .....	5
2.2 Histology .....	6
2.3 Gastrointestinal Motility.....	7
2.4 Theoretical Modeling.....	8
2.5 Intraluminal Pressure Measurement.....	8
2.6 Contact Force Measurement.....	10
Chapter 3: Methods .....	13
3.1 Surgical Methods.....	13
3.2 Design Requirements .....	15
3.3 MFS Device Characterization.....	16
3.4 MFS Device Validation.....	18
3.5 Porcine Studies .....	19
3.6 Human Studies.....	20
Chapter 4: Results .....	22
4.1 Design Modifications .....	22
4.2 MFS Device Characterization.....	28
4.3 MFS Device Validation.....	29
4.4 Porcine Studies .....	36
4.5 Human Studies.....	38

Chapter 5: Conclusion .....	46
Appendices .....	51
Appendix A: MFS Balloon Fabrication Procedure .....	51
Appendix B: MFS Gasket Fabrication Procedure .....	53
Appendix C: Material Data Sheet for Silicone Dispersion .....	56
Appendix D: SolidWorks Part Drawings for MFS Hub Fabrication .....	57
Appendix E: LabVIEW Code Used to Operate the Syringe Pump .....	59
Appendix F: Matlab Code Used for MFS Characterization.....	60

# List of Tables

Table 1: Gender, age, weight, and method of anesthesia for all four patients included in the study. ....	21
Table 2: Characterization coefficients ( $c_1 - c_5$ ), $R^2$ from regression testing ( $R^2$ Fit), and $R^2$ from characterization and validation ( $R^2$ Validate) used for all four human studies. Balloon 1 is nearest the trailing cap (see Fig 11). ....	29
Table 3: Comparison of pressure step response percent difference between two pre-operative trials (Test 1-2) and two post-operative trials (Test 3-4). ....	34
Table 4: Mean contact force response for a 1N load placed on each balloon. ....	36
Table 5: Porcine myenteric contact force per cm axial length. ....	38
Table 6: Myenteric contact force results for the human small bowel. ....	44

# List of Figures

Figure 1: PillCam® SB (Given Imaging Ltd.) .....	2
Figure 2: Migrating Motor Complex Force Sensor (MFS) used by Terry <i>et al.</i> [4-6].	11
Figure 3: Full setup used by Terry <i>et al.</i> to collect porcine myenteric contact force data.....	11
Figure 4: 12 mm diameter trocar port used for laparoscopic procedures.....	14
Figure 5: Roux-En-Y Gastric Bypass procedure (Blaussen Medical Imaging, Inc.). The Y junction provides an ideal location for MFS insertion. ....	15
Figure 6: Characterization chamber and flat plate used for the characterization of each balloon.....	17
Figure 7: Validation setup. A 100 g weight is placed on each balloon for one minute. ....	19
Figure 8: LabVIEW VI used to control MFS inflation, deflation, and data collection for the human study. ....	23
Figure 9: MFS complete with all human modifications.....	24
Figure 10: MFS inside its sterile packaging, ready for human study.....	25
Figure 11: MFS resting in its holder. The MFS is also sterilized while in the holder. The numbers 1-4 are used to reference each balloon. Balloon 4 is nearest the leading cap. ....	26
Figure 12: Method for <i>in vivo</i> height compensation. A laser is projected across the top of the MFS holder and onto the patient. The surgeon then measures the difference between this point and the <i>in vivo</i> position of the MFS. ....	27
Figure 13: Hollow tube attached to an <i>ex vivo</i> pneumatic pressure sensor used to measure insufflation pressure. The trocar is mostly hidden from view.....	28
Figure 14: Inflation (I), deflation (II), and re-inflation (III) of a typical MFS balloon with respect to time. Note the pressure decay associated with sections I and III....	31
Figure 15: Side by side comparison of Sections I and III from Figure 14. Note the similar pressure decays between the two. ....	32

Figure 16: Typical pressure measurements for all four MFS balloons. The balloons are inflated for eight minutes, deflated for five minutes, and then re-inflated for eight minutes. Note the stepped response in Section C..... 34

Figure 17: Comparison of old balloon design with new, smaller design used for human studies..... 37

Figure 18: Full MFS data collection setup in the human OR..... 39

Figure 19: MFS in sterile field during its initial inflation. On the right side of the table is the ruler used for hydrostatic pressure compensation and lubricant applied to the deflated MFS immediately before insertion into the trocar. .... 40

Figure 20: Surgeon applying lubricant to the deflated MFS just prior to trocar insertion. .... 41

Figure 21: MFS insertion into the human abdominal cavity through a 12 mm trocar. .... 41

Figure 22: MFS as it enters the abdominal cavity through the trocar. In this image the MFS is still in a deflated state..... 42

Figure 23: Inflated MFS inside the human small bowel..... 43

Figure 24: Myenteric contractile response of the human small bowel from a single MFS with four balloon segments. .... 44

Figure 25: Balloon molds being dipped into silicone dispersion..... 52

Figure 26: Balloon molds being rotated..... 52

Figure 27: Metal spear piercing the MFS gasket..... 53

Figure 28: PTFE tube inserted through the hub and gasket..... 54

Figure 29: Gasket seated on the hub ready for a balloon to be attached. .... 55

# Chapter 1: Introduction

## 1.1 Motivation

Proper functionality of the human digestive system is essential for sustaining life. Numerous disorders are known to be associated with the system due to its complex nature. The small intestine in particular may have abnormalities ranging from Crohn's and Celiac disease to intestinal cancer. According to the Centers for Disease Control and Prevention, the most common cancer associated with the digestive system is colorectal cancer, which ranks as the third most common cancer among both men and women in the United States. In 2010, 52,045 people died from colorectal cancer, making it the second deadliest cancer that affects both men and women [1]. Early detection is crucial for the successful treatment of digestive carcinomas.

The current standard of care for the diagnosis of digestive disorders is through direct observation and biopsy of the digestive tract using flexible endoscopy. A small fiber optic camera attached to a long flexible tube is inserted either into the mouth or the anus to inspect the upper and lower gastrointestinal tracts, respectively. While this technique is suitable to access the esophagus, stomach, and colon, the small bowel remains difficult to access with this method. To

overcome this obstacle, capsule endoscopy was introduced and has been approved for use in the United States since 2001. Manufactured by Given Imaging, the 11 mm x 26 mm PillCam® SB (Fig 1) features a tiny camera inside a clear capsule that when swallowed by the patient, records intraluminal images as it passes through the digestive tract. This type of capsule endoscopy is limited however, because it passively moves through the patient's digestive tract with peristalsis; making the capsule unable to intentionally stop for a prolonged diagnosis [2].

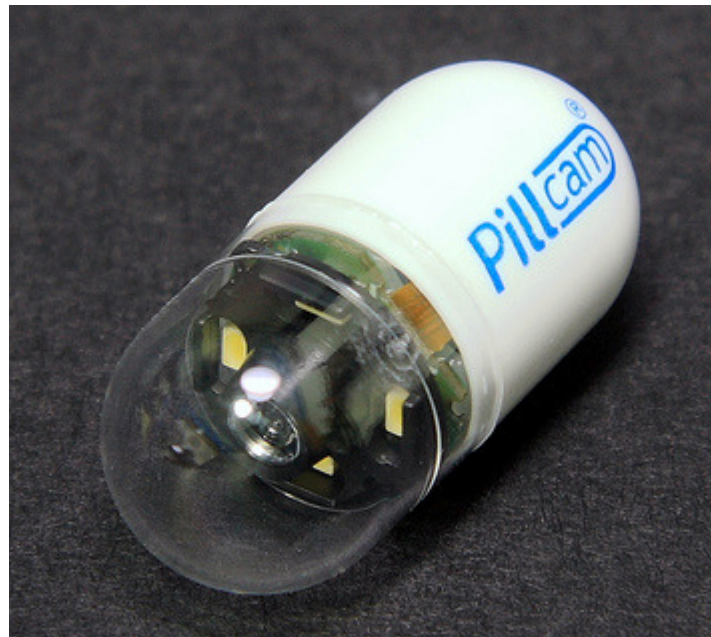


Figure 1: PillCam® SB (Given Imaging Ltd.)

As a crucial next step, capsule endoscopes which can be controlled and maneuvered by the physician are currently under investigation. These experimental devices collectively known as robotic capsule endoscopes (RCE) combine the natural orifice, minimally invasive benefit of traditional endoscopy with the nimbleness of

an untethered, maneuverable device. Such a device may potentially benefit not only diagnostic procedures, but also may provide therapeutic applications [3].

The human body provides a challenging environment for a robotic capsule endoscope. First, the device must be of a sufficient size and shape that it is swallowable. Next, it must resist the corrosive and varying pH levels throughout the gastrointestinal tract. Finally, the RCE needs sufficient power and traction that it can successfully overcome the convoluted geometry, tribological properties, and *in vivo* forces associated with the intraluminal environment.

## 1.2 Scope

This study focuses on the mechanical characterization of the small intestine, specifically active peristaltic forces. This region of the gastrointestinal tract is selected because it is the most difficult region to access through traditional natural orifice techniques and therefore will benefit the most from robotic capsule endoscope technology.

The *in vivo* forces associated with the intraluminal environment of the small intestine are related to the biomechanical response of the tissue, mucus adhesivity, tribology, and active peristaltic forces. Terry *et al.* developed a suite of test devices to better understand and characterize these phenomena [4-6]. They consist of a biaxial test apparatus and method for characterizing the biomechanical properties of the duodenum, jejunum, and ileum, a novel *in vitro* device and protocol designed to measure the energy required to overcome the self-adhesivity of the mucosa, a novel tribometer that measures the *in vivo* coefficient of friction between the mucus

membrane and the robot surface, and finally, a novel manometer and force sensor array that measure force per axial length generated by the migrating motor complex (MMC) .

Data gathered for the active force generated by the migrating motor complex using the manometer and force sensor array was done so in a live porcine model with an open surgical technique in a non-sterile environment. This protocol is not suitable for data collection in a live human due to the invasiveness of the procedure and risk of infection. Therefore, the goal of this study is to measure the active myenteric contraction force of the small bowel against a solid bolus in a human by modifying the force sensor array used by Terry *et al.* [4-6] so that it uses a minimally invasive, sterile surgical technique.

## Chapter 2: Background

The human gastrointestinal tract is accessible through two natural orifices: the mouth and the anus. For a robotic capsule endoscope to access the small intestine utilizing either of these natural orifices, it must maneuver through the esophagus and stomach or the rectum and large intestine. The following chapter discusses the anatomy and motility of the small intestine as well as research conducted to measure intraluminal pressure and contact force of the small intestine against a solid bolus.

### 2.1 Gross Anatomy

The small intestine is a hollow tube approximately six to seven meters long [7]. It consists of three functional regions, the duodenum, jejunum, and ileum. Traveling in the aboral direction, the duodenum is the first region of the small intestine. It is separated from the stomach by the pyloric orifice. Usually 20-25 cm in length, its lumen is the widest of any section of the small intestine [7]. The duodenum features secretory glands and is important in the mixing of gastric chyme with pancreatic and biliary secretions. Continuing in the aboral direction, the jejunum is the middle region of the small intestine and is the primary site for

nutrient absorption. It is characterized by prominent circular folds which slow intestinal transit of chyme while simultaneously increasing the absorptive surface area [8]. The most distal section of the small bowel is known as the Ileum. It has the smallest lumen diameter, thinnest walls, and least vascularization of any anatomical region of the small intestine. The jejunum and ileum are attached to the posterior abdominal wall by the mesentery which also supplies vascularization to the organ and nutrient transport from the organ [7].

## **2.2 Histology**

Four layers of tissue: the mucosa, submucosa, muscularis externa, and serosa form the intestinal wall. The mucosa layer is the inner most; facing the lumen. Circular folds referred to as plicae and small finger-like projections called villi characterize this area. A thin layer of smooth muscle named the muscularis mucosa moves the villi back and forth in a sweeping motion which helps facilitate nutrient absorption and dispersion of protective mucus. The muscularis mucosa is innervated by the submucosal plexus which is located within the submucosa (the next layer in the intestinal wall moving from the lumen). Beyond this layer, the muscularis externa contains two layers of smooth muscle responsible for GI motility. They consist of an inner circular layer and an outer longitudinal layer, both innervated by the myenteric plexus which lies between them. Finally, an outer layer of connective tissue called the serosa helps protect the intestine [9].

### **2.3 Gastrointestinal Motility**

Motility in the small intestine derives from a complex interaction of smooth muscle tissue. The longitudinal muscle of the muscularis externa shortens the small bowel while the circular muscle predominantly facilitates pressure gradients. These pressure gradients provide the driving force that propels intestinal contents aborally [10].

In general, the small intestine exhibits three patterns of motor activity. The first two patterns discussed are present in the postprandial phase of digestion. Peristalsis results from circular muscle contraction immediately behind a bolus which propels it in the aboral direction. This is the primary means by which intestinal contents travel through the digestive tract. Moving from the duodenum to the distal ileum, transit of intestinal contents slows [10]. The other characteristic motor activity present in the human postprandial response is segmental contractions. Alternating segments of small bowel contract and relax which churn intestinal contents while at the same time producing no net movement of the contents.

The third pattern of GI motility is only present during fasting. A series of contractions originating in the stomach propagate to the large intestine over the span of approximately 90 minutes. Collectively referred to as the migrating motor complex (MMC), it is thought to serve a housekeeping function that sweeps indigestible materials and bacteria out of the stomach and small bowel and into the large intestine [9]. The activity of the MMC usually exhibits three wave patterns. Phase I is marked by motor quiescence, phase II displays irregular contractions,

and phase III is marked by dense, rhythmic, high amplitude contractions [11]. An RCE requires an *in vivo* environment similar to this fasting motility so that the intestinal wall can be visualized without being obscured by intestinal contents. Therefore, an accurate measurement of the active contact forces generated by the MMC against a solid bolus such as a RCE is crucial for its development. The distinction of a solid bolus is necessary because the small intestine usually contains liquid bolus.

## 2.4 Theoretical Modeling

Currently, the contact force exerted by the small intestine against a solid bolus has not been experimentally measured in a human. The nearest estimates of this force in the literature come from theoretical modeling of intestinal tissue. Early work by Bertuzzi *et al.* established a general theoretical model for peristaltic transport of a solid bolus [12]. More recent work by Miftahof *et al.* focused on the development of theoretical models of solid bolus transport within the gastrointestinal tract [13-14]. They estimate axial contact force produced by the intestinal wall around a solid, non-deformable bolus to vary from 0.15 to 1.9 N/cm.

## 2.5 Intraluminal Pressure Measurement

Most of what is known about gastrointestinal motility comes from direct measurement of intraluminal pressure. Early work used a technique known as balloon-kymography to measure intraluminal pressure of the stomach, duodenum, and jejunum in humans [15]. This technique had a tendency to produce an

exaggerated index of motor activity and resulted in the development of open-tipped catheters which proved a more stable method to measure intraluminal pressures [16].

Current motility research based on intraluminal pressure measurement utilizes two types of manometry: water perfused or solid state. In water perfused manometry, intraluminal pressure waves are translated to *ex vivo* pressure transducers through open-tipped catheters as water is perfused through the catheter system by a pump. This method of measurement is cheaper than its solid state counterpart and can record more sites simultaneously which increases sensor resolution [17-19]. However, since this method uses a water filled tube, it is limited by the laws of fluid dynamics and is sensitive to changes in height due to hydrostatic pressure. Additionally, large catheter diameters associated with water perfused systems may interfere with progression of the MMC in the aboral direction [20].

Solid-state manometry features *in vivo* pressure transducers which permit the patient to remain ambulatory during data collection. Data can be gathered continuously over the span of several days to produce a more accurate profile of the patient's motility. Additionally, since fluid dynamics are not involved with solid-state manometry, a faster frequency response is available; though this is more beneficial for the upper GI than it is for small bowel studies [21]. *In vivo* pressure transducers do however considerably increase the system cost while decreasing the durability and ease of sterilization.

The small intestine is difficult to reach through natural orifices using tradition manometry. Therefore, most manometric motility research is focused on the esophagus, stomach and large intestine. Seidl *et al.* used a solid-state manometry array to measure the fasting MMC motility and postprandial response of the human jejunum and ileum in ten healthy volunteers. They measured mean MMC Phase III contraction amplitude to be  $3.84 \pm 0.1$  kPa in the jejunum and a mean contraction propagation velocity of  $1.4 \pm 0.1$  cm/s [11].

## 2.6 Contact Force Measurement

Although the manometric pressures throughout the GI tract are generally understood, no previous work has measured these intraluminal pressures against a solid bolus or equated the pressure readings to actual contact force values in a human. Terry *et al.* [4-6] developed a novel manometer and force sensor array and corresponding characterization method that measured force per cm axial length generated by the MMC in a porcine small intestine. The sensor, hereafter referred to as the Migrating Motor Complex Force Sensor (MFS) featured multiple torus shaped balloons; each connected to an *ex vivo* pressure transducer (Fig 2-3). Corresponding temperature measurements were recorded for each balloon and a perfused manometer recorded the abdominal pressure.

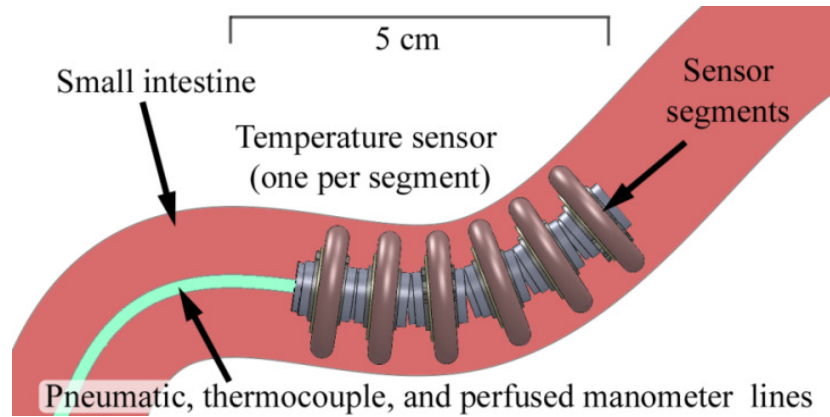


Figure 2: Migrating Motor Complex Force Sensor (MFS) used by Terry *et al.* [4-6].

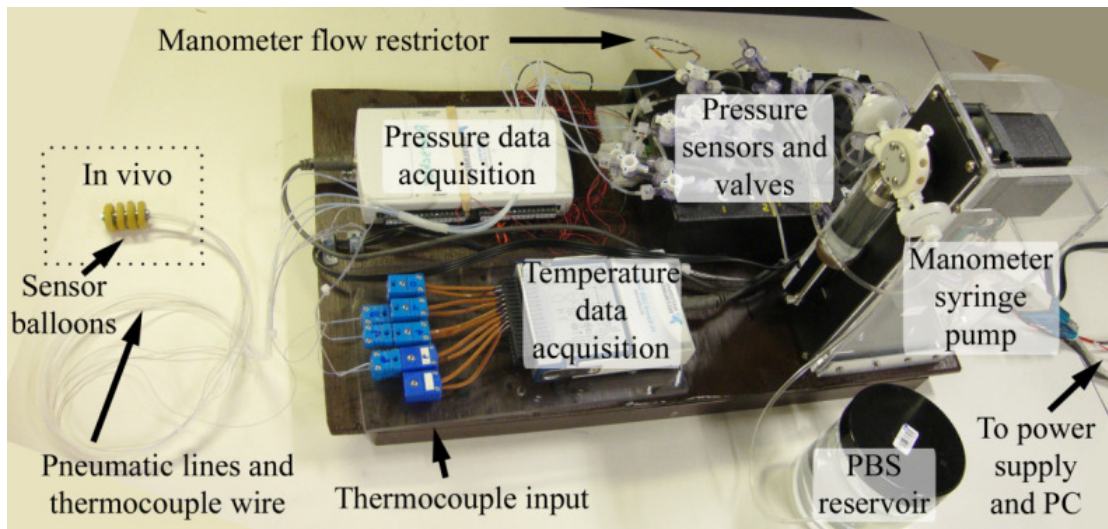


Figure 3: Full setup used by Terry *et al.* to collect porcine myenteric contact force data.

Placing two sensors in a single porcine model, they measured a mean contact force of  $1.34 \pm 0.14$  N/cm and  $1.18 \pm 0.22$  N/cm in the medial and distal regions of the small bowel, respectively [4-6]. As a follow up to their original study, Terry *et al.* used the same sensor to measure proximal, middle, and distal regions of the small intestine in multiple live porcine models. Their results yielded an average contact

force value of  $1.9 \pm 1.0$  N/cm with distal force measurements generally higher than proximal values. As a crucial next step, this study aims to modify the sensor developed by Terry *et al.* to enable the first ever measurement of myenteric contact force against a solid bolus in a human small intestine.

## **Chapter 3: Methods**

### **3.1 Surgical Methods**

Surgical access to the human abdominal cavity is traditionally achieved through a large incision referred to as a laparotomy. As surgical techniques advance, more procedures previously performed by laparotomy are now performed using a minimally invasive technique called laparoscopy. This technique avoids a large incision and instead employs several small incisions through which hollow tubes known as trocars are placed (Fig 4). The trocar maintains a pathway into the peritoneal cavity which is inflated with CO<sub>2</sub> gas to separate the abdominal wall from the internal organs. The surgeon visualizes the abdominal cavity with the use of a small camera called a laparoscope which is inserted through one of the trocars. The remaining trocars act as a conduit for surgical instruments. This minimally invasive surgical technique reduces the risk of infection and also reduces patient recovery time.



Figure 4: 12 mm diameter trocar port used for laparoscopic procedures.

Roux en-Y Gastric Bypass surgery is one such procedure that is increasingly performed by laparoscopy. For this operation, the patient is placed under general anesthesia while the superior portion of the stomach nearest the base of the esophagus is segmented into a small pouch which serves as the patient's new stomach. The small intestine is transected and attached to this new pouch. The duodenum is then attached to the jejunum at the Y-junction allowing the patient's original stomach to drain into the GI tract (Fig 5). The Roux en-Y Gastric Bypass serves as an excellent candidate procedure for MFS implantation. Just before the duodenum is attached at the Y-junction, the MFS is inserted through one of the 12 mm trocars, into the jejunum at the Y-junction in the aboral direction. Once in place, the MFS gathers myenteric contact force data for approximately five minutes before it is removed from the patient. By using patients already undergoing a

gastric bypass surgery, no extra incisions are required and the patient is already under general anesthesia. The only patient impact is an additional five minutes added to the approximately two hour Roux en-Y procedure time.

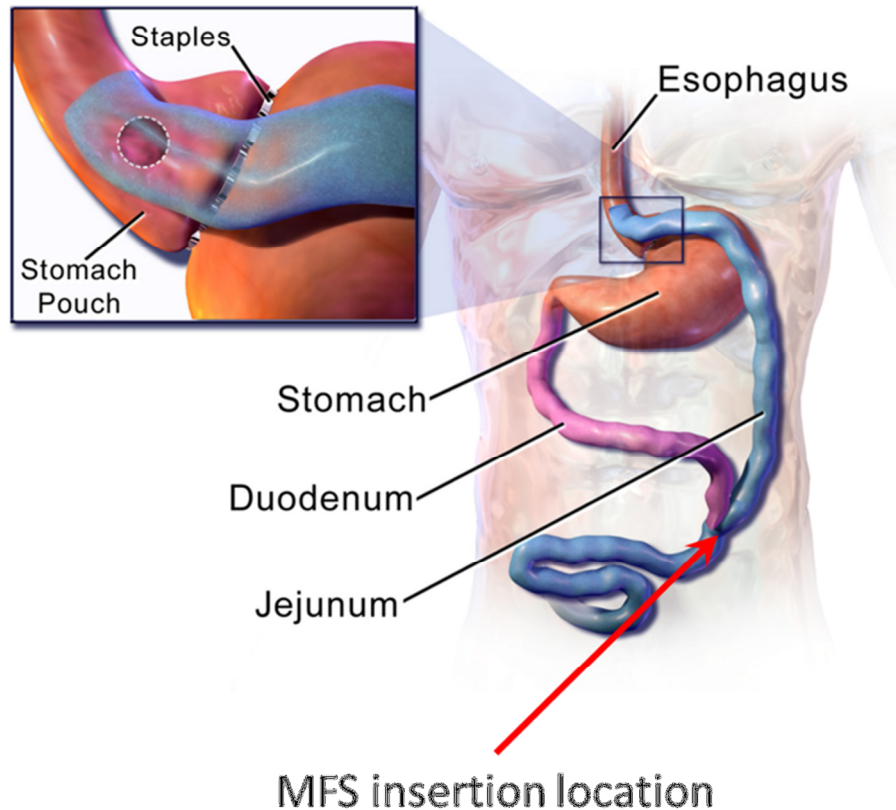


Figure 5: Roux-En-Y Gastric Bypass procedure (Blausen Medical Imaging, Inc.). The Y junction provides an ideal location for MFS insertion.

### 3.2 Design Requirements

Previous porcine myenteric contact force measurements gathered by Terry *et al.* using the MFS were done so with an open surgical technique by laparotomy.

Changing to a laparoscopic technique in a human introduces multiple design requirements. First, the MFS must fit into and out of the 12 mm diameter trocar while being maneuvered by the surgeon within the abdominal cavity using a surgical grasper. Next, the MFS must be constructed from materials that are known to be biocompatible in a human and capable of sterilization. It is imperative that the MFS is sterile before it is inserted into the patient. Finally, any research involving human test subjects must be approved by the organization's Institutional Review Board (IRB).

### 3.3 MFS Device Characterization

In order to convert intraluminal pressures recorded by the MFS into myenteric contact force data, each balloon on the MFS must be characterized. An applied force ( $F_c$ ), temperature ( $T_a$ ), and ambient pressure ( $P_a$ ) provide a known input while the internal pressure for each balloon ( $P_s$ ) serves as a measured output. Terry *et al.* proved that radial contact loading was not necessary for MFS characterization [4-6]. Instead they use a flat plate to contact each balloon at three distinct locations ( $L_c$ ). The same characterization procedure is employed for this study with the exception that the balloons are filled with deionized water instead of air.

The contact force ( $F_c$ ) is derived empirically as a function of sensor pressure ( $P_s$ ), ambient pressure ( $P_a$ ), ambient temperature ( $T_a$ ), and contact location ( $L_c$ )

$$F_c = c_1 L_c^2 + c_2 L_c + c_3 \Delta P_s + c_4 \Delta P_a + c_5 \Delta T_a \quad (3.1)$$

The constants  $c_1 - c_5$  represent the characterization coefficients that are unique to each balloon. A custom chamber and mounting fixture (Fig 6) are designed to simulate *in vivo* conditions through the variation of ( $F_c$ ), ( $P_s$ ), ( $P_a$ ), ( $T_a$ ), and ( $L_c$ ).

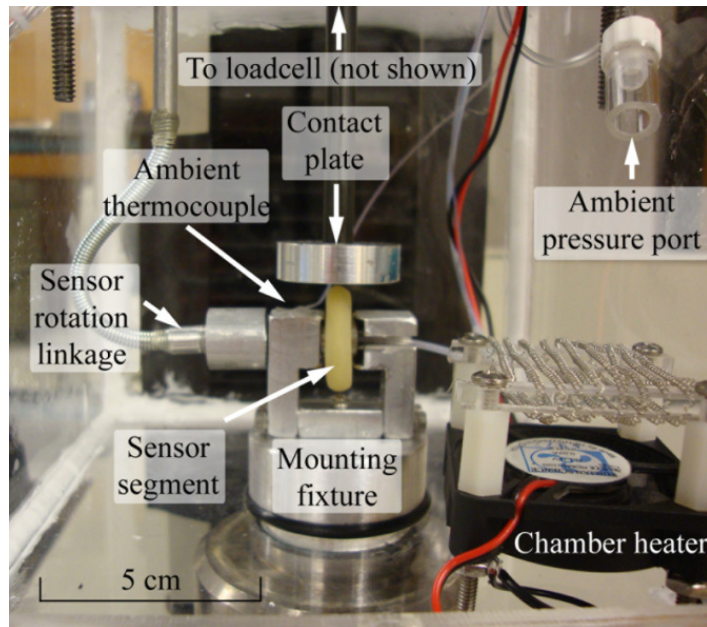


Figure 6: Characterization chamber and flat plate used for the characterization of each balloon.

Each balloon is characterized using the following method: 1) The balloon is mounted in the characterization chamber and inflated to an internal pressure ( $P_s$ ) of 14 kPa for eight minutes. 2) The chamber temperature ( $T_a$ ) is varied at four discrete values between room temperature and 37°C while the gage pressure inside the chamber ( $P_a$ ) is varied between 0 and 2 kPa to simulate the insufflated abdomen. 3) At a rate of 1 mm/s, a flat aluminum plate attached to a 5 N loadcell (PN 100-090-674, MTS Systems Corporation) is brought into contact with the balloon. The plate

continues to contact the balloon until it is within 2 mm of its rigid central hub following which; it is retracted at the same rate. The plate contacts the balloon three consecutive times after which the balloon is rotated 120° and then 240° for another three contacts per location. Changing the contact location (0°, 120°, and 240°) is necessary to account for any variation in wall thickness of the hand-made balloons. 4) Steps 2 and 3 are repeated until all permutations of temperature, pressure, and contact location are achieved. 5) The balloon is then left to sit for eight additional minutes until it is deflated. Balloon pressure, chamber temperature, chamber pressure, contact location, contact force, and flat plate displacement are sampled at 50Hz and recorded using LabVIEW Signal Express throughout the duration of the characterization. The data is supplied to (3.1) to solve for the characterization coefficients  $c_1 - c_5$ ; unique to each balloon.

### **3.4 MFS Device Validation**

Of the data gathered during the characterization procedure, half is used to calculate the characterization coefficients  $c_1 - c_5$  while the other half of the data is used to validate those values. As an additional step, a secondary validation procedure is added to this study while the MFS is in its fully assembled configuration. Inflation and deflation of the MFS balloons is actuated by the syringe pump and LabVIEW software. 1) The fully assembled MFS is initially inflated to 14 kPa and left to sit for eight minutes. 2) The balloons are deflated for five minutes to simulate MFS insertion through the trocar and into the small bowel. 3) The MFS is then re-inflated for eight minutes during which a 100 gram weight is placed

successively on each balloon for a duration of one minute per balloon (Fig 7). The characterization coefficients  $c_1 - c_5$  are used to calculate the force placed on each balloon.

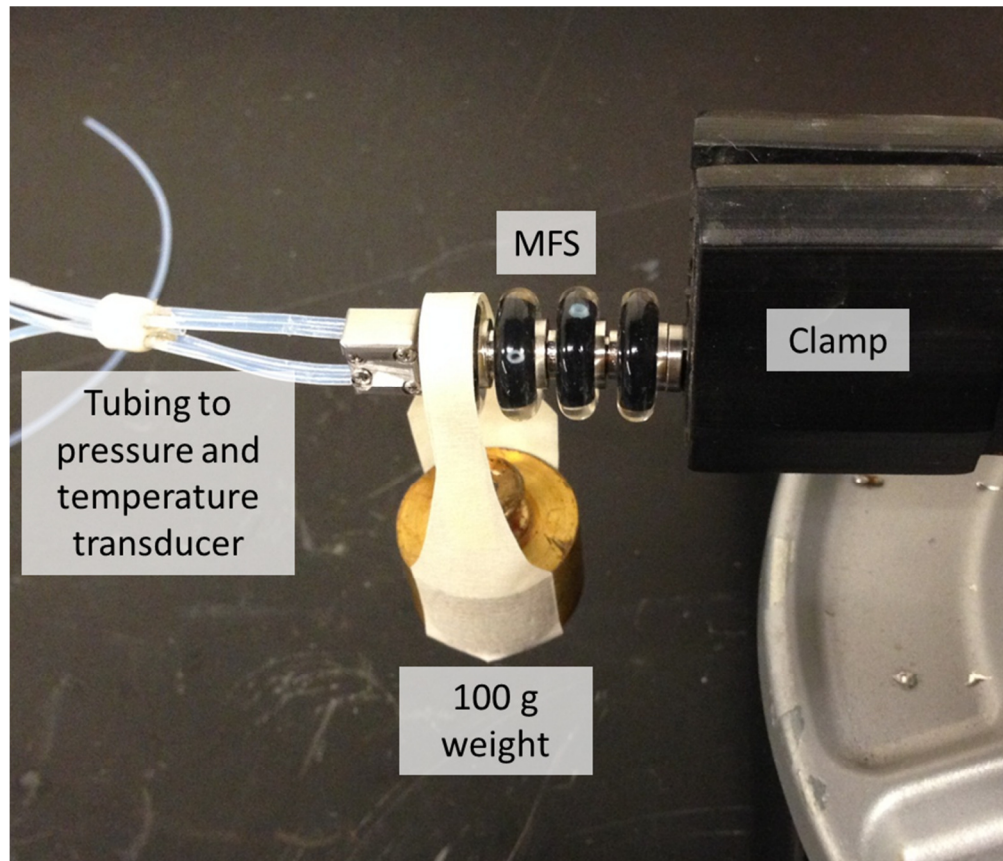


Figure 7: Validation setup. A 100 g weight is placed on each balloon for one minute.

### 3.5 Porcine Studies

The MFS is tested in four different live porcine models prior to human testing. Each porcine study serves as practice for the human study and allows the surgeon to give feedback for successive design iterations. All pigs included in the study are standard female ranging in age from 6-12 months and weighing 120-130

lbs. A bowel preparation prior to surgery is administered to each pig ensuring that the small intestine is clear of any material. Starting 48 hours prior to surgery, the pig is fed nothing but water and Jell-O® and then only water the final 24 hours. Additionally, an agent that removes all intestinal worms is given to the pig two days prior to surgery. All pigs are generally anesthetized using Ketamine as the anesthetic agent and Xylazine for sedation. Atropine and Glycopyrrolate are avoided as anesthetic agents because they are known to reduce GI motility. Concluding data collection, the pig is humanly euthanized in accordance with Institutional Animal Care and Use Committee (IACUC protocol 87912(04)1D) regulations.

The general test procedure for each porcine study is to inflate the MFS to 14 kPa and let it sit for 10 minutes. The sensor is then deflated for five minutes while it is inserted into the porcine small bowel. Following this, all balloons are re-inflated and data is collected for a period of 10 minutes.

### **3.6 Human Studies**

Institutional Review Board (IRB) approval is received (COMIRB Protocol 11-0157) for MFS data collection in up to five patients. All patients included in this study are slated for Rou-en-Y gastric bypass surgery and give informed, written consent before they are included in the study. The MFS is implanted in a total of four patients: three females and one male ranging from 27 to 69 years of age (Table 1). One day prior to surgery, each patient ingests a series of laxatives and consumes only clear liquids to ensure that the small intestine is clear of any matter. The

patients in the first and second studies are anesthetized by desflurane gas while those included in the third and fourth studies receive intravenous (IV) remifentanil. The remifentanil is stopped 10 minutes prior to MFS implantation and resumed after data collection is complete in an effort to elucidate the effects of anesthesia on GI motility.

Table 1: Gender, age, weight, and method of anesthesia for all four patients included in the study.

Study	Gender	Age	Weight (Kg)	Anesthesia
1	Female	27	130	Desflurane gas
2	Female	35	120	Desflurane gas
3	Male	69	125	Remifentanil IV
4	Female	68	120	Remifentanil IV

Due to time constraints within the operating room (OR), data collection time for all human studies is five minutes. Since the final version of the MFS used for human testing is dependent on the results of the human compatible MFS design requirements, more detail of the MFS human surgical implantation procedure is presented in Section 4.5. In general, the human procedure is as follows: 1) The MFS is inflated to 14 kPa for eight minutes. 2) The balloons are then deflated for five minutes. 3) The MFS is re-inflated for eight minutes. 4) Steps 1-3 are repeated a total of five times. During the third time, the surgeon inserts the MFS into the small bowel and step three serves as the actual *in vivo* data collection. Data from *in vivo* human experiments is used to calculate the mean contact force for each human and balloon.

## Chapter 4: Results

### 4.1 Design Modifications

The inflated MFS (22 mm diameter) is too large to fit through the 12 mm diameter trocar. Therefore it must be deflated before it is inserted into the abdomen. To accomplish this, a custom LabVIEW Virtual Instrument (VI) is used to sequentially inflate all balloons of the MFS to a user defined value at a user defined rate (typical values are 14 kPa and 1 ml/min). The program then deflates the balloons at a rate and fixed volume specified by the user. Finally, a re-inflation command is used to add the exact volume removed for deflation back into each balloon at the same previous rate. Pressure and temperature are recorded at 50 Hz using a National Instruments USB-6218 and 9213 data acquisition system (DAQ), respectively. The same deflation command is then used once more to remove the MFS from the patient. Inflation and deflation of each balloon is performed by a syringe pump (P/N 736935A, Cavro Scientific Instruments, Inc.). The user controls designed to operate the MFS are displayed in Figure 8. Real time balloon pressures and temperature are displayed as well as commands for initial inflation, deflation, and re-inflation.

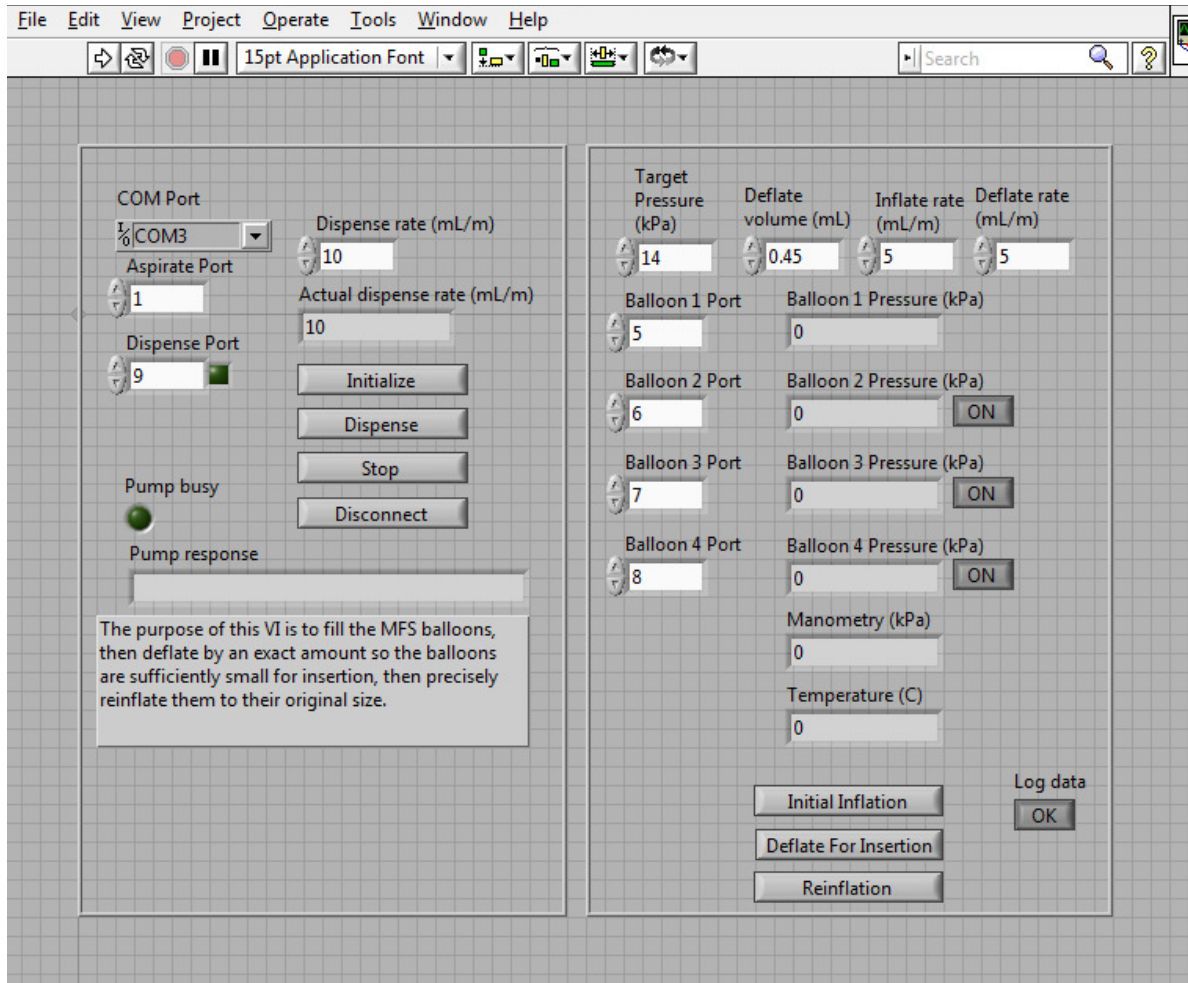


Figure 8: LabVIEW VI used to control MFS inflation, deflation, and data collection for the human study.

To provide a location for the surgeon to maneuver the MFS *in vivo*, a cap is added to the leading and trailing side of the MFS. This cap enables the surgeon to safely grasp the MFS with a laparoscopic instrument while averting any damage to the delicate balloons.

Bio compatibility is achieved by switching the previously used latex balloons with medical grade silicone (MED 2014, NuSil Technology, LLC.). Additionally, the central mounting hub and washer for each balloon is constructed from medical

grade stainless steel (316 LVM SS). This same material is used to construct the leading and trailing caps. The 0.032 in (inner diameter) polytetrafluoroethylene (PTFE) tubing remains unchanged since it is known to be biocompatible. The final, human compatible version of the MFS is presented in Figure 9.

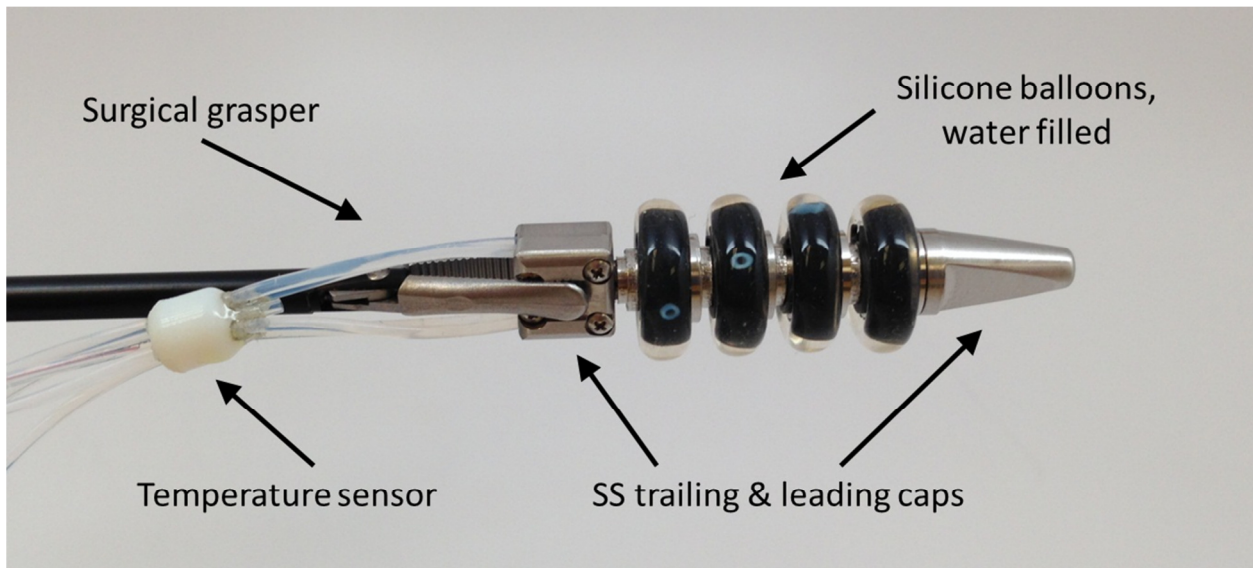


Figure 9: MFS complete with all human modifications.

Sterility of the MFS is of chief concern for the human study. To execute this, the MFS is packaged and placed inside a low temperature sterilization machine (STERRAD®) where it is sterilized by hydrogen peroxide ( $H_2O_2$ ) gas (Fig 10). The post-sterilized MFS successfully maintains balloon pressurization and a separate *in vitro* validation is conducted using previously sterilized balloons (Section 4.3).

Inside the OR, the MFS is unwrapped by the surgeon and placed on a sterile table. To maintain a sterile field, the PTFE tubing and thermocouple length must be increased from three feet to ten feet. This allows enough tubing for the implanted

MFS to be connected to its *ex vivo* pressure transducers and DAQ outside of the sterile field. Increased tubing length adds a potentially time consuming hazard for the surgeon. To reduce the likelihood of tangled tubing within the sterile pack, small couplers are employed to keep the tubing together. One such coupler is visible in Figure 9. A custom holder that protects the MFS while it is *ex vivo* is implemented to act as a weighted base which prevents the tension developed by the additional tubing length from inadvertently pulling the MFS off the sterile table during surgical use (Fig 11).



Figure 10: MFS inside its sterile packaging, ready for human study.

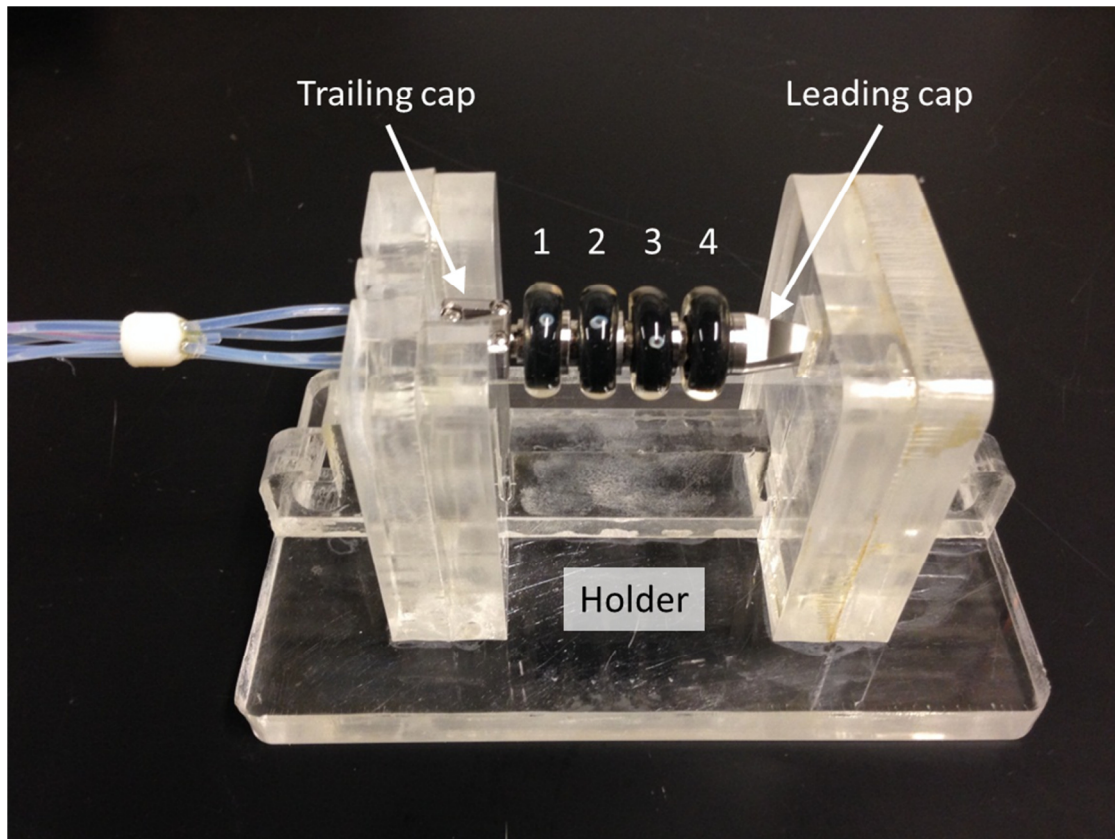


Figure 11: MFS resting in its holder. The MFS is also sterilized while in the holder. The numbers 1-4 are used to reference each balloon. Balloon 4 is nearest the leading cap.

Throughout the duration of data collection, the *ex vivo* pressure transducers remain stationary while the *in vivo*, water filled tubing and balloons of the MFS vary in height relative to the pressure transducers. This introduces a hydrostatic effect present in the *in vivo* data. Previous versions of the MFS compensated for this by measuring the change in height ( $\Delta h$ ) between the height the MFS was initially inflated at and the *in vivo* height of the sensor. This same principle is employed for height compensation in the human study; however the technique must not contaminate the sterile field. To achieve this, a laser pointer is utilized to establish the height of the MFS holder relative to the patient. The surgeon then estimates the

*in vivo* height of the sensor and measures the difference between the *in vivo* height and the laser point with a sterile ruler, thus establishing  $\Delta h$ .

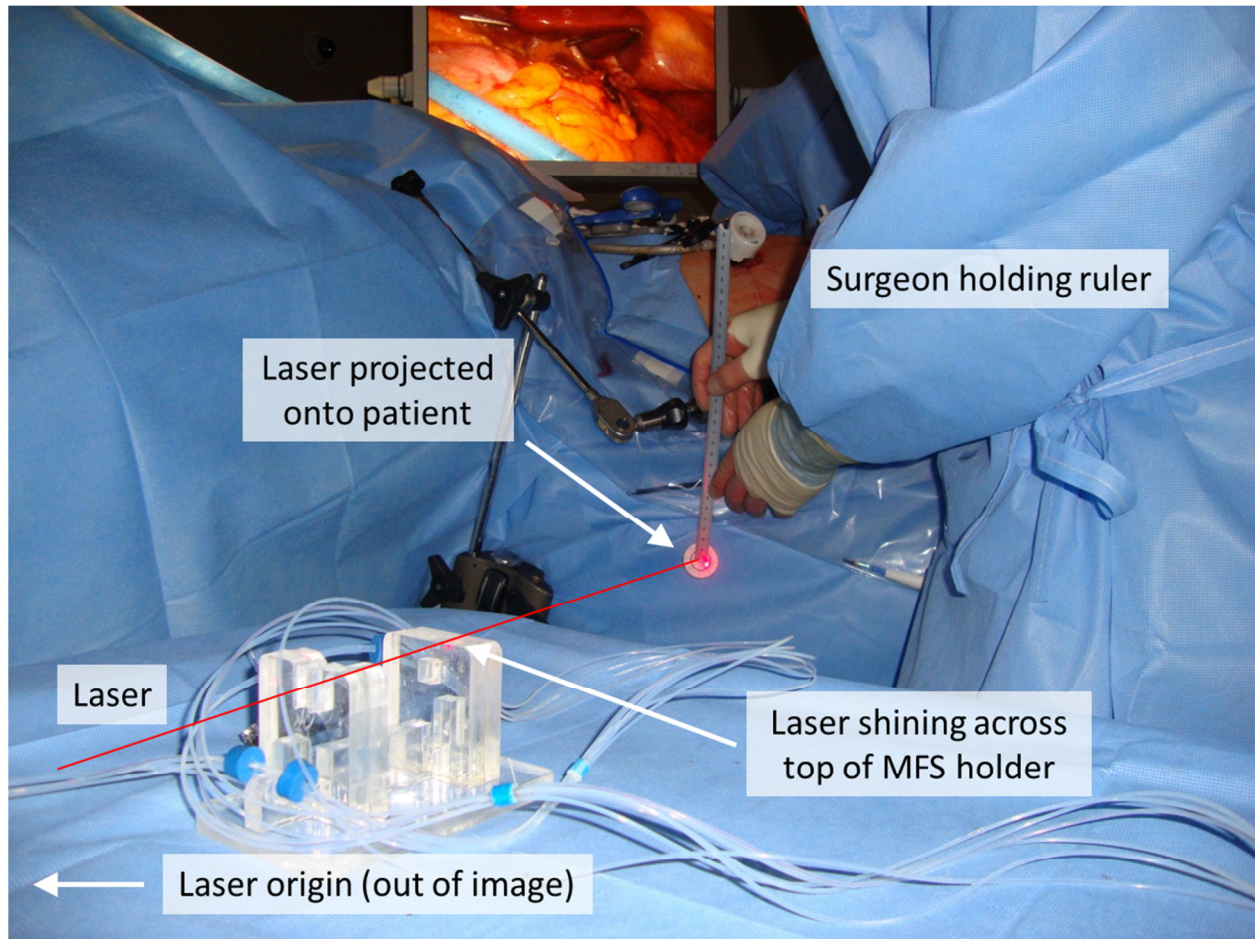


Figure 12: Method for *in vivo* height compensation. A laser is projected across the top of the MFS holder and onto the patient. The surgeon then measures the difference between this point and the *in vivo* position of the MFS.

One final design modification for sterility is the method by which abdominal pressure is recorded. Terry *et al.* used a perfused manometer system which pumped phosphate buffered saline (PBS) into the porcine abdomen. Using this same method in a human contaminates the sterile field. Therefore, a new technique is implemented where a small hollow tube connected to an *ex vivo* pressure transducer

is inserted through the trocar. The open end of the tube is suspended in the open space of the CO<sub>2</sub> filled abdominal cavity (Fig 13). Insufflation pressure ( $P_a$ ) is then recorded for the duration of *in vivo* data collection using an *ex vivo* pneumatic pressure sensor.

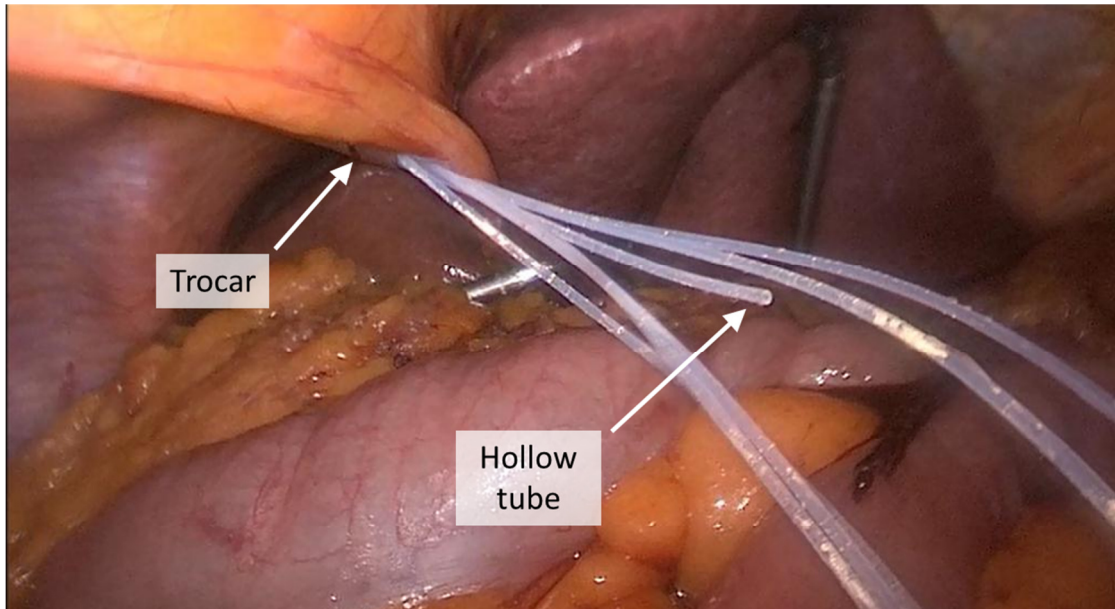


Figure 13: Hollow tube attached to an *ex vivo* pneumatic pressure sensor used to measure insufflation pressure. The trocar is mostly hidden from view.

Finally, the Institutional Review Board (IRB) approves the MFS to be implanted in up to five human subjects provided each patient signs a written consent (COMIRB Protocol 11-0157).

#### 4.2 MFS Device Characterization

Characterization results for all balloons used in the human studies are listed in Table 2. The mean  $R^2$  from regression testing ( $R^2$  Fit) is  $0.90 \pm 0.07$  and the mean

$R^2$  from characterization and validation ( $R^2$  Validate) is  $0.89 \pm 0.07$ . No balloons were used more than twice for human testing.

Table 2: Characterization coefficients ( $c_1 - c_5$ ),  $R^2$  from regression testing ( $R^2$  Fit), and  $R^2$  from characterization and validation ( $R^2$  Validate) used for all four human studies. Balloon 1 is nearest the trailing cap (see Fig 11).

Human Study	Balloon	$R^2$ Validate	$R^2$ Fit	$c_1$	$c_2$	$c_3$	$c_4$	$c_5$
1	1	0.8379	0.8507	-0.0912	0.3378	0.4294	-0.2903	-0.0101
	2	0.6918	0.7212	-0.081	0.3545	0.4215	-0.3306	-0.0174
	3	0.8934	0.9048	-0.0194	0.0777	0.4515	-0.3241	-0.0001
	4	0.917	0.9246	-0.0375	0.1834	0.4586	-0.3088	-0.0188
2	1	0.9282	0.9329	-0.0571	0.2196	0.4154	-0.3219	-0.0105
	2	Same Balloon 2 used in Human Study 1						
	3	Same Balloon 3 used in Human Study 1						
	4	Same Balloon 4 used in Human Study 1						
3	1	0.8979	0.9078	-0.0566	0.2455	0.4674	-0.3515	-0.0118
	2	0.9185	0.9241	-0.0276	0.1297	0.4492	-0.3363	-0.0038
	3	0.9418	0.9473	-0.0169	0.1062	0.4213	-0.2765	0.0051
	4	0.8447	0.8579	-0.0679	0.2893	0.413	-0.2747	-0.0154
4	1	Same Balloon 1 used in Human Study 2						
	2	0.8676	0.8737	-0.0667	0.2872	0.4376	-0.3514	-0.0283
	3	0.9268	0.9348	-0.0533	0.2171	0.4296	-0.303	-0.0128
	4	0.9621	0.9655	-0.0357	0.1485	0.4047	-0.2911	-0.0081

### 4.3 MFS Device Validation

The validation presented in Table 2 is calculated from the characterization data. An additional validation and method for data analysis of the MFS in its fully assembled configuration is presented here. The approach used to evaluate the validation data is also used to analyze data from human subjects.

When an MFS balloon is inflated to 14 kPa and left to rest, it exhibits stress relaxation. The volume of the balloon expands over time resulting in a gradual decrease in balloon pressure. The phenomena can be seen graphically in Figure 14, Section I. The stress relaxation is abrupt at first, but then becomes linear after several minutes. The stress relaxation is disrupted, however, when the balloon is deflated for insertion into the human small bowel (Fig 14, Section II). The pressure during the deflated period remains constant because the pressure transducer is closed; protecting it from the vacuum of deflation. The pressure spikes displayed points B and C are there to serve as a data marker; done so by pinching the MFS tubing near the pressure transducer. Once the balloon is re-inflated, the pressure transducer is re-opened and the balloon pressure continues to decay (Fig 14, Section III). A nearly identical stress relaxation is observed comparing the pressure profile of Section I to that of Section III (Fig 15); the fact of which is used in the following data analysis.

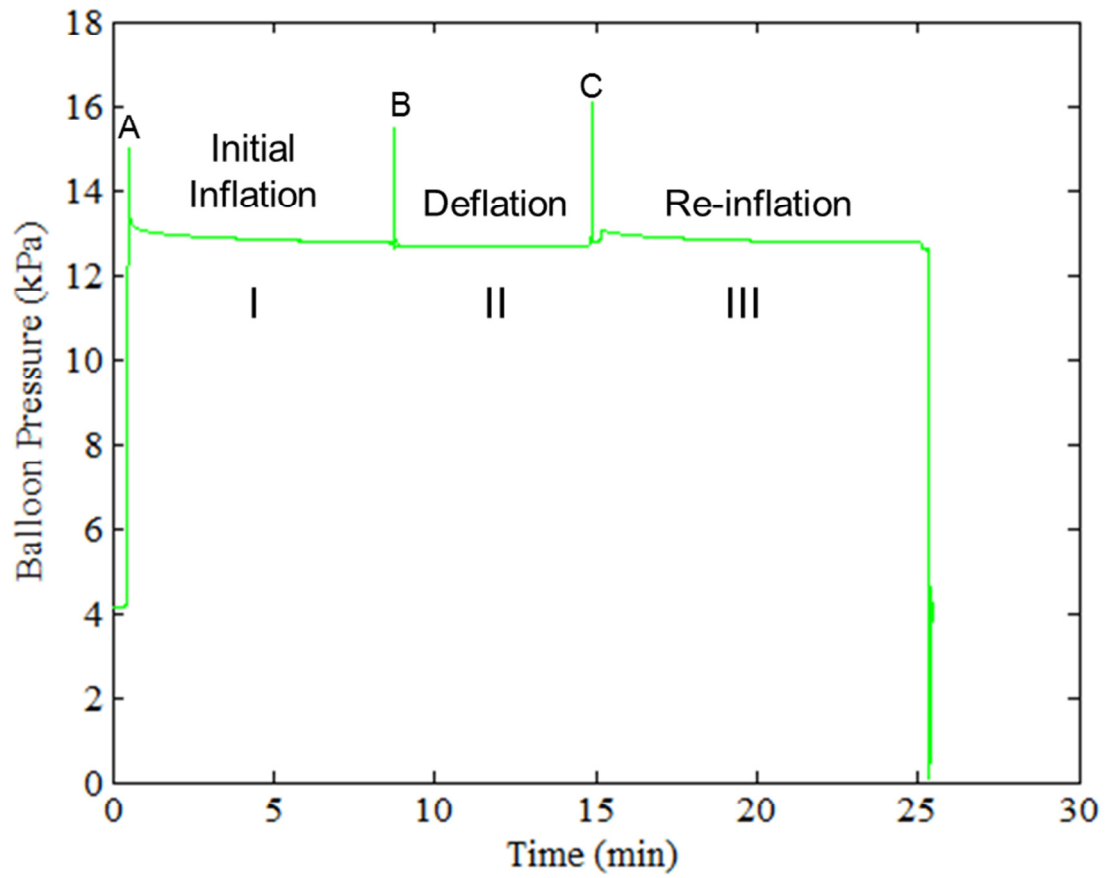


Figure 14: Inflation (I), deflation (II), and re-inflation (III) of a typical MFS balloon with respect to time. Note the pressure decay associated with sections I and III.

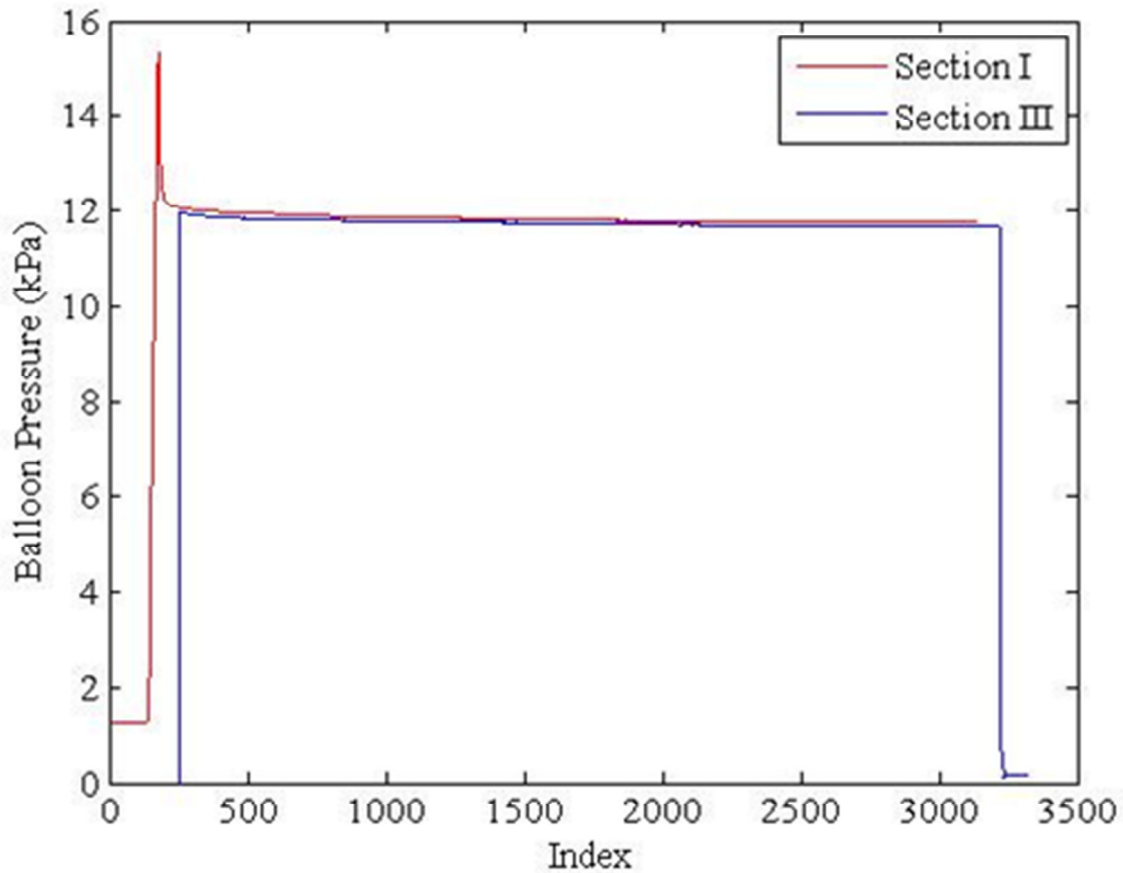


Figure 15: Side by side comparison of Sections I and III from Figure 14. Note the similar pressure decays between the two.

One final consideration is the effect the syringe pump has on the re-inflated balloon pressure. The result of inflating all four balloons for eight minutes, deflating for five minutes, then re-inflating for eight minutes can be seen in Figure 16. Although the stress relaxation rates are the same for each balloon between Section III and its corresponding Section I value, the offset of the pressure curve is different in Section III compared to its initial value in Section I. After investigating the issue, this stepped response appears to be originating from the syringe pump itself. One possible explanation is that a tiny amount of air is entering the system as the

stepper motor contained within the syringe pump cycles through the multiple ports used in the inflation and deflation process. To compensate for this, multiple inflation-deflation cycles are performed immediately prior to and following a human study. The 2000<sup>th</sup> data point on the pressure curve after the initial inflation data spike and re-inflation data spike are compared to measure the step value. These points are chosen arbitrarily because they are near the midway point of data collection. The step response is then evaluated as the percent difference between those two points. The percent difference is averaged between two pre-operative and two post-operative inflation-deflation trials in the OR and used to predict the *in vivo* step response. An example of the percent differences observed for the syringe pump step response is shown in Table 3.

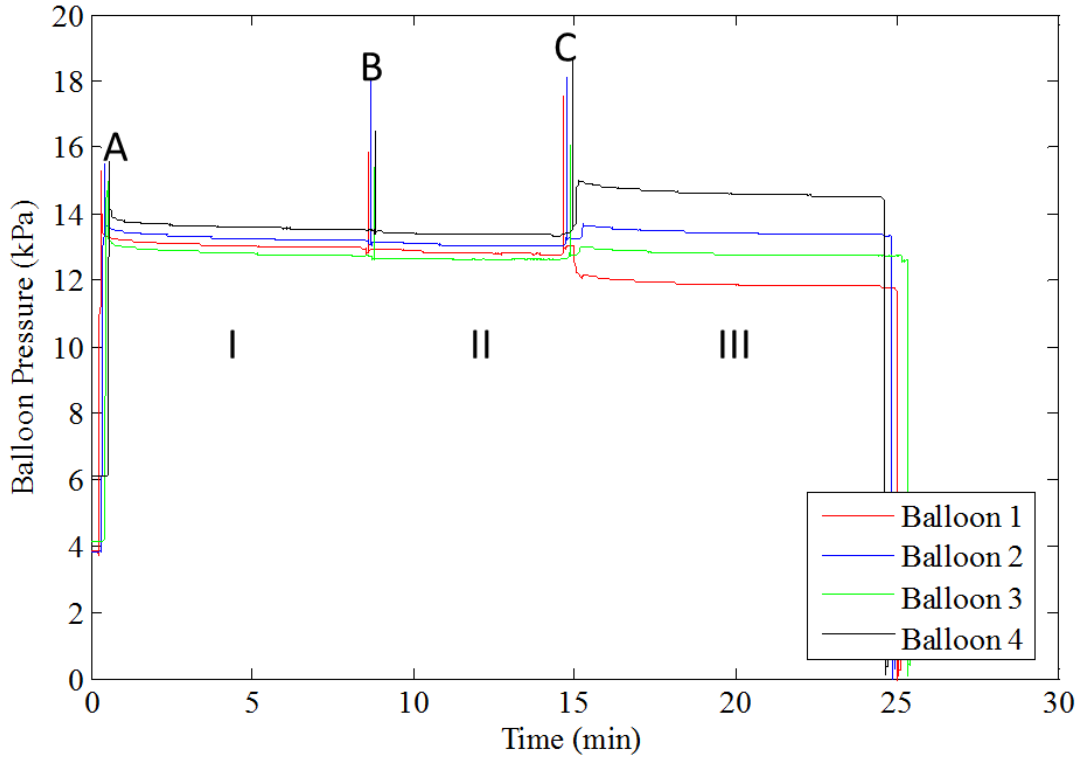


Figure 16: Typical pressure measurements for all four MFS balloons. The balloons are inflated for eight minutes, deflated for five minutes, and then re-inflated for eight minutes. Note the stepped response in Section C.

Table 3: Comparison of pressure step response percent difference between two pre-operative trials (Test 1-2) and two post-operative trials (Test 3-4).

Test	Percent Difference Balloon 1	Percent Difference Balloon 2	Percent Difference Balloon 3	Percent Difference Balloon 4
1	0.9273	0.9956	1.0101	1.0846
2	0.9189	0.9954	0.9893	1.0753
3	0.9107	1.0129	1.0000	1.0753
4	0.9031	1.0090	0.9886	1.0765
Average	0.9150	1.0032	0.9970	1.0779

With these considerations in mind, the validation and human study data analysis method may be discussed. First, the initial inflation and *in vivo* portions of

the MFS pressure curve are identified ( $P_{initial}$ ) and ( $P_{in vivo}$ ), respectively. Next, subtracting the change in pressure due to the *in vivo* height of the MFS from ( $P_{in vivo}$ ) gives ( $P_{in vivo,height adj}$ ). Multiplying the average percent difference of the syringe pump step response ( $c_{syringe}$ ) by ( $P_{initial}$ ) gives a tare line ( $P_{tare}$ ) with the same pressure decay as the *in vivo* data. This line represents a reference point of zero MFS contact force.

$$P_{tare} = c_{syringe} * P_{initial} \quad (4.1)$$

Next, subtracting ( $P_{tare}$ ) from ( $P_{in vivo,height adj}$ ) gives the change in intraluminal pressure due to contact force ( $\Delta P_s$ ).

$$\Delta P_s = P_{tare} - P_{in vivo,height adj} \quad (4.2)$$

Supplying ( $\Delta P_s$ ) into (3.1) along with ( $P_a$ ), ( $T_a$ ), ( $L_c$ ), and characterization coefficients  $c_1 - c_5$  defined previously, yields the conversion of intraluminal pressure to contact force.

The results of the validation are displayed in Table 4. Each balloon is independently subjected to a 1N force. Balloon two appears to have a smaller than expected mean force value because the syringe pump response ( $c_{syringe}$ ) did not accurately predict the pressure tare line ( $P_{tare}$ ).

Table 4: Mean contact force response for a 1N load placed on each balloon.

Balloon	Mean contact force (N)
1	$1.02 \pm 0.02$
2	$0.73 \pm 0.02$
3	$1.01 \pm 0.02$
4	$1.03 \pm 0.02$

#### 4.4 Porcine Studies

Initial porcine testing demonstrated that the MFS was too large to fit into and out of the trocar without damaging the delicate sensor. The friction caused by the leading balloons (B1, B2) sliding through the trocar during MFS insertion caused them to pull slightly from their stainless steel hubs; breaking their seal which caused them to not hold sufficient pressure *in vivo*. In addition, as the deflated MFS was removed from the small bowel and pulled back out through the trocar, the trailing balloons (B1, B2) caught on the sharp, *in vivo* end of the trocar. In one case, the balloon was fully stripped from the MFS but was retrieved from the pig's abdominal cavity by the surgeon.

Each balloon is made by dipping a custom aluminum mold into a silicone dispersion, rotating it for several hours and then repeating for a total of three dips. Following this process, the silicone coated molds are baked in an oven at 150°C for two hours. To allow the balloons to fit more easily into and out of the trocar, new aluminum balloon molds are created that reduce the balloon diameter by 5 mm (Fig 17). Additionally, by increasing the curvature of the outer edge of each mold, the balloon is functional with an overall reduction in wall thickness because the silicone

disperses more evenly around the molds. Previously, three coats of silicone were used to ensure that the characteristic “weak spot” (Fig 17) was thick enough to hold a nominal balloon pressure of 14 kPa. The new balloons only require two dips in the silicone to function with the same nominal operating pressure.

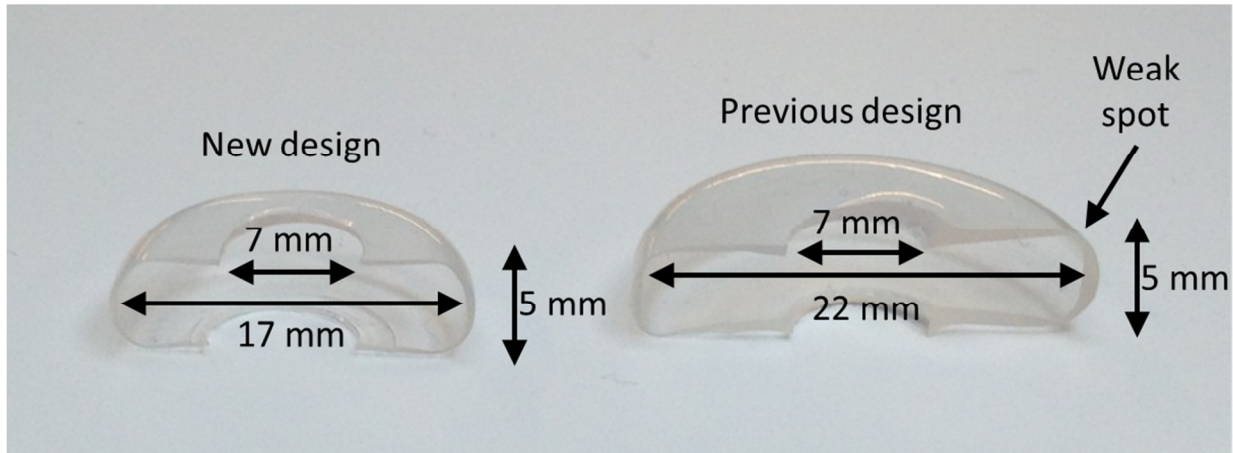


Figure 17: Comparison of old balloon design with new, smaller design used for human studies.

An additional lesson learned from the porcine studies is the difficulty involved with threading the PTFE tubing through the stainless steel trailing cap. In several of the early porcine studies, the PTFE tubing kinked inside the trailing cap and in some cases was cut by it. This issue lessened over time as the author developed the tactile response necessary to tighten the trailing cap without kinking or cutting the balloons.

The average porcine myenteric contact force is  $1.20 \pm 0.08$  N/cm which is slightly less than that observed by Terry *et al.* Individual averages for each balloon in the final porcine study are displayed in Table 5.

Table 5: Porcine myenteric contact force per cm axial length.

Balloon	Contact Force [N/cm]
1	$1.91 \pm 0.08$
2	$1.69 \pm 0.06$
3	$1.76 \pm 0.06$
4	$1.83 \pm 0.13$

#### 4.5 Human Studies

The full MFS data collection setup in the human OR is displayed in Figure 18. The MFS is seated in its holder and placed on a sterile table. The PTFE tubing extends from the MFS to the *ex vivo* pressure transducer and data acquisition system. A more detailed picture of the sterile portion of the MFS can be seen in Figure 19.

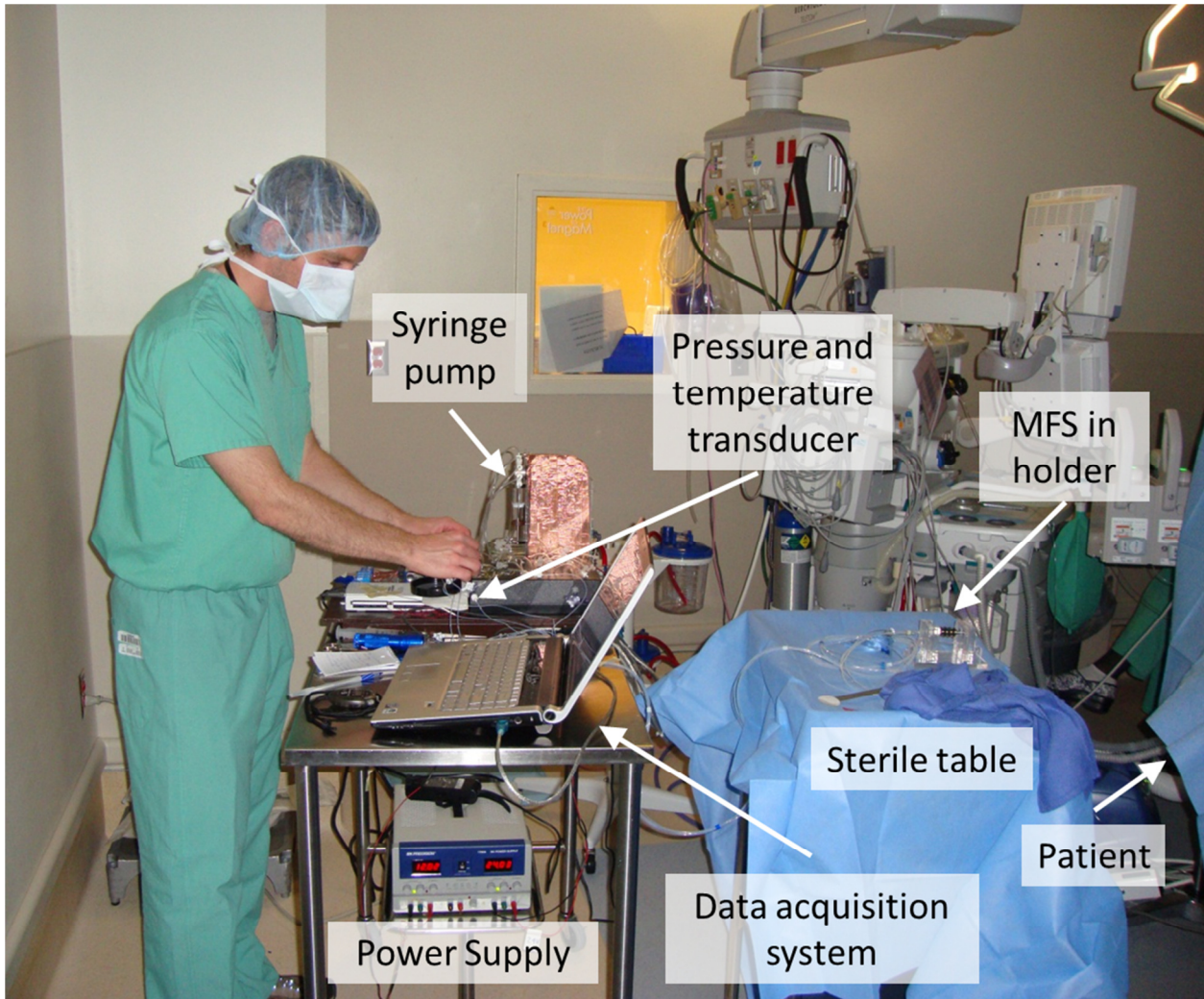


Figure 18: Full MFS data collection setup in the human OR.

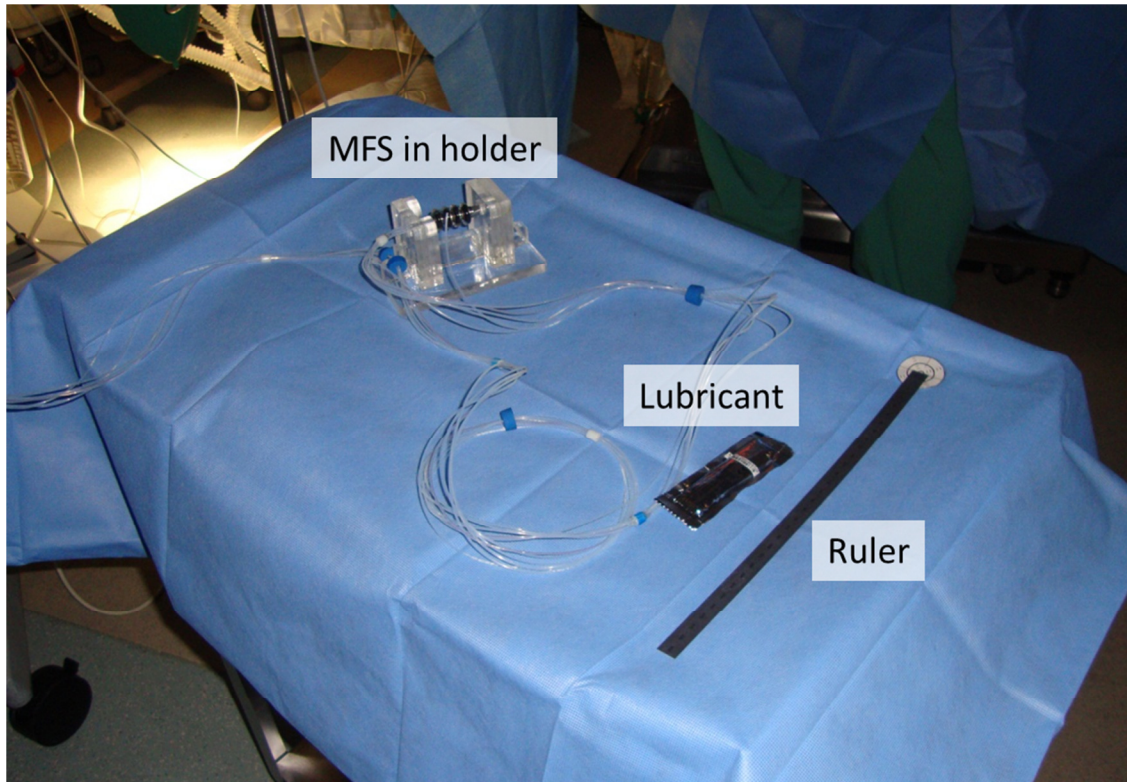


Figure 19: MFS in sterile field during its initial inflation. On the right side of the table is the ruler used for hydrostatic pressure compensation and lubricant applied to the deflated MFS immediately before insertion into the trocar.

Once the surgeon unwraps the MFS from its sterile packaging and all connections are established with the *ex vivo* system outside the sterile field, the MFS is inflated to 14 kPa for eight minutes. It is then deflated for five minutes and re-inflated for eight minutes. This cycle is repeated two more times except that re-inflation occurs *in vivo* during the third cycle. Once the MFS is removed from the patient, it is returned to its holder where it undergoes two additional cycles of eight minutes inflation, five minutes deflation, and eight minutes re-inflation as it sits on the sterile table. The surgeon applies lubricant onto the MFS (Fig 20) prior to inserting it into the trocar with a surgical grasper (Fig 21).

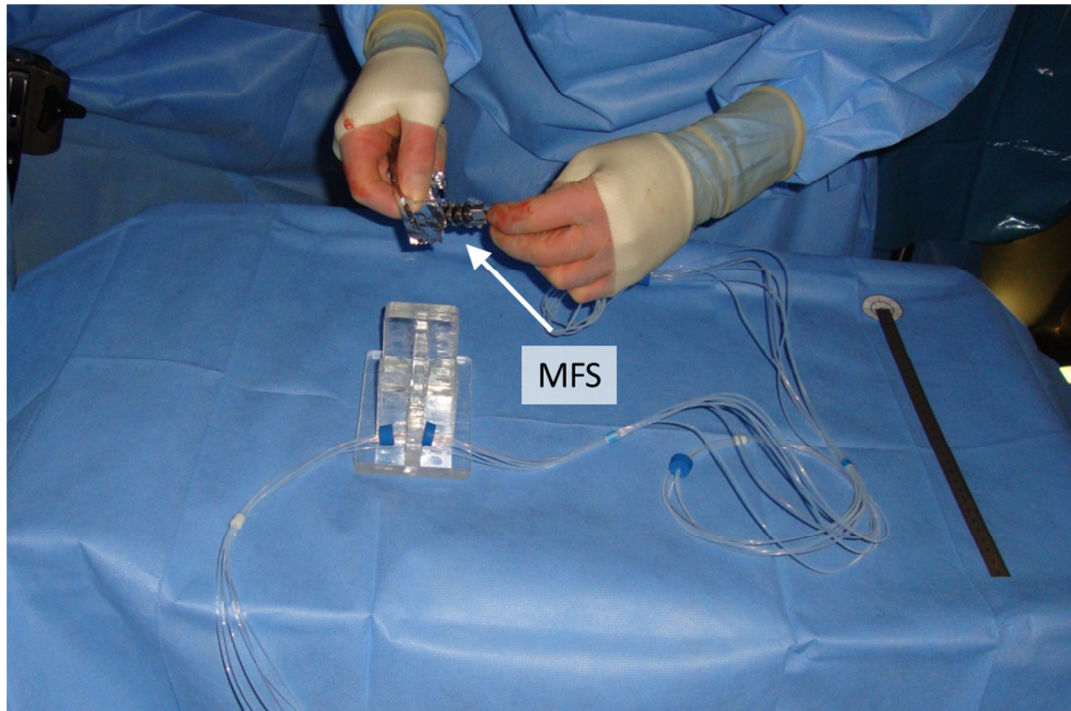


Figure 20: Surgeon applying lubricant to the deflated MFS just prior to trocar insertion.

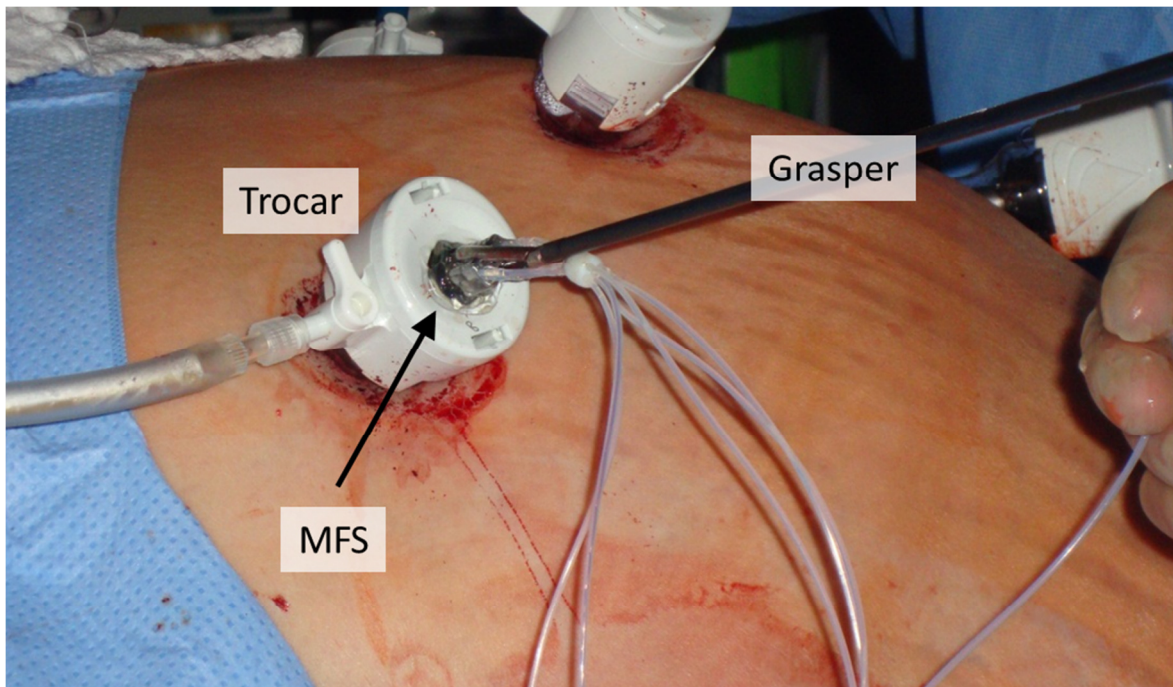


Figure 21: MFS insertion into the human abdominal cavity through a 12 mm trocar.

The MFS enters the abdominal cavity (Fig 22) and is finally inserted into the jejunum. The small, hollow tube used to measure abdominal insufflation pressure is inserted through the trocar and left suspended in the CO<sub>2</sub> pressurized abdominal cavity (Fig 13). The MFS is then re-inflated to collect myenteric contact force data for approximately five minutes (Fig 23).

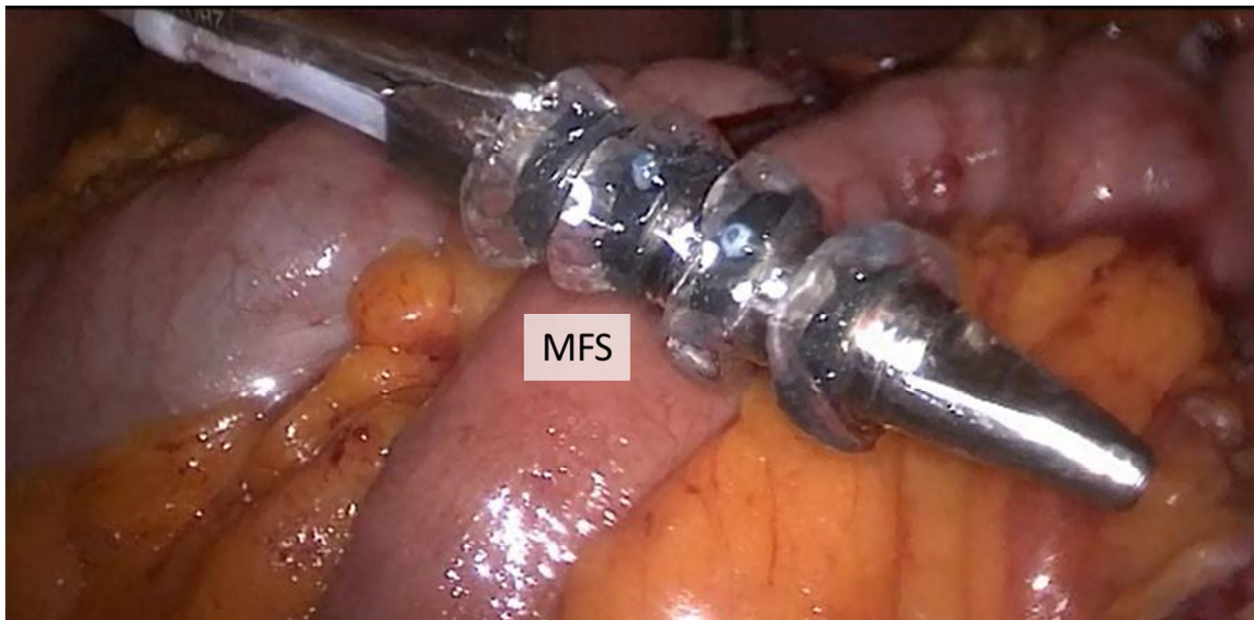


Figure 22: MFS as it enters the abdominal cavity through the trocar. In this image the MFS is still in a deflated state.

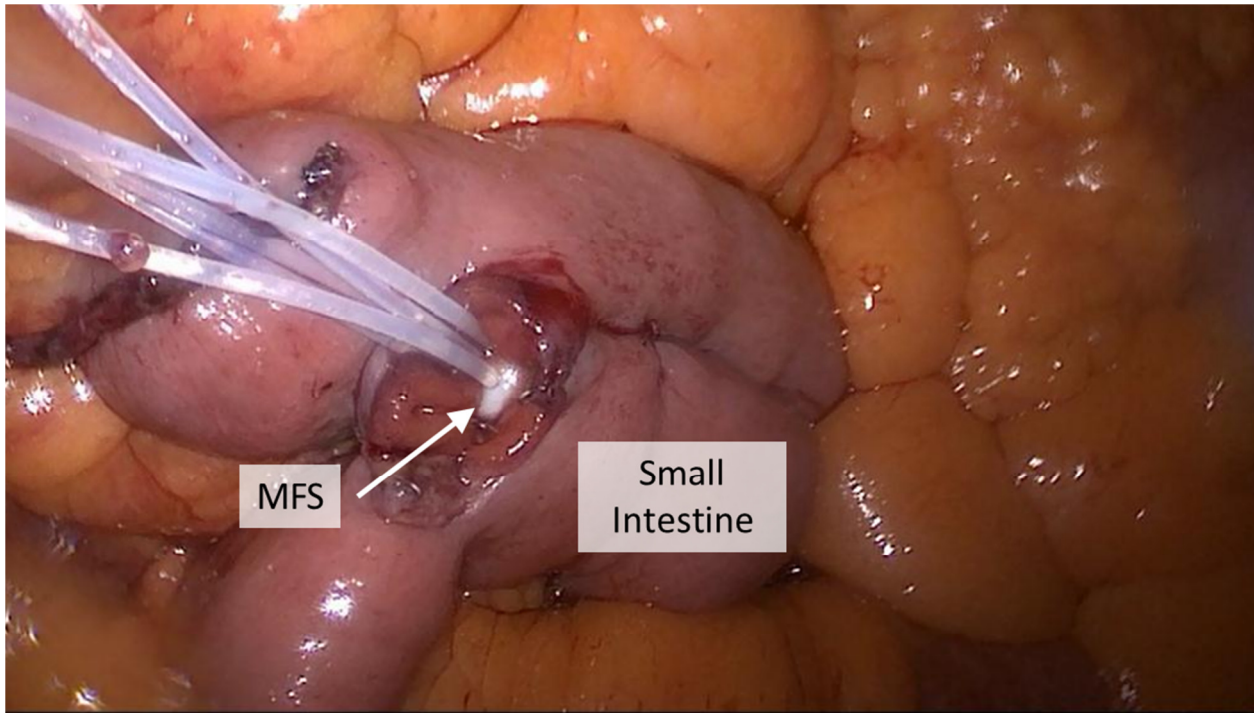


Figure 23: Inflated MFS inside the human small bowel.

Results of the four human studies are summarized in Table 6. The average contact force for all four patients is  $0.03 \pm 0.55$  N/cm. The patients for the first and second studies received desflurane gas anesthesia. Little if any peristalsis was measured from these first two so the third and fourth studies received total intravenous (IV) anesthesia which is shorter acting and believed to have a lesser effect on peristalsis. In the third and fourth study, the IV anesthesia (remifentanyl) was stopped 10 minutes prior to MFS insertion and resumed once data collection was complete. Peristalsis around the MFS was clearly visualized for the patient in the third study but could not be visualized for the fourth because the small bowel remained hidden behind other tissue for the duration of data acquisition. The small bowel was easily visualized for the first and second patients, however no peristalsis

was observed. A plot of contraction force versus time for the third study is displayed in Figure 24.

Table 6: Myenteric contact force results for the human small bowel.

Balloon	Study 1 [N/cm]	Study 2 [N/cm]	Study 3 [N/cm]	Study 4 [N/cm]
1	$0.17 \pm 0.02$	$0.11 \pm 0.05$	$0.47 \pm 0.05$	$0.08 \pm 0.01$
2	$-0.21 \pm 0.03$	$-0.03 \pm 0.06$	$0.79 \pm 0.05$	$-1.66 \pm 0.01$
3	$0.43 \pm 0.01$	$0.64 \pm 0.03$	$1.37 \pm 0.05$	$-0.78 \pm 0.01$
4	$-0.62 \pm 0.03$	$-0.43 \pm 0.07$	$0.21 \pm 0.06$	$-0.13 \pm 0.06$
Average	$-0.06 \pm 0.14$	$0.07 \pm 0.07$	$0.71 \pm 0.05$	$-0.62 \pm 0.02$

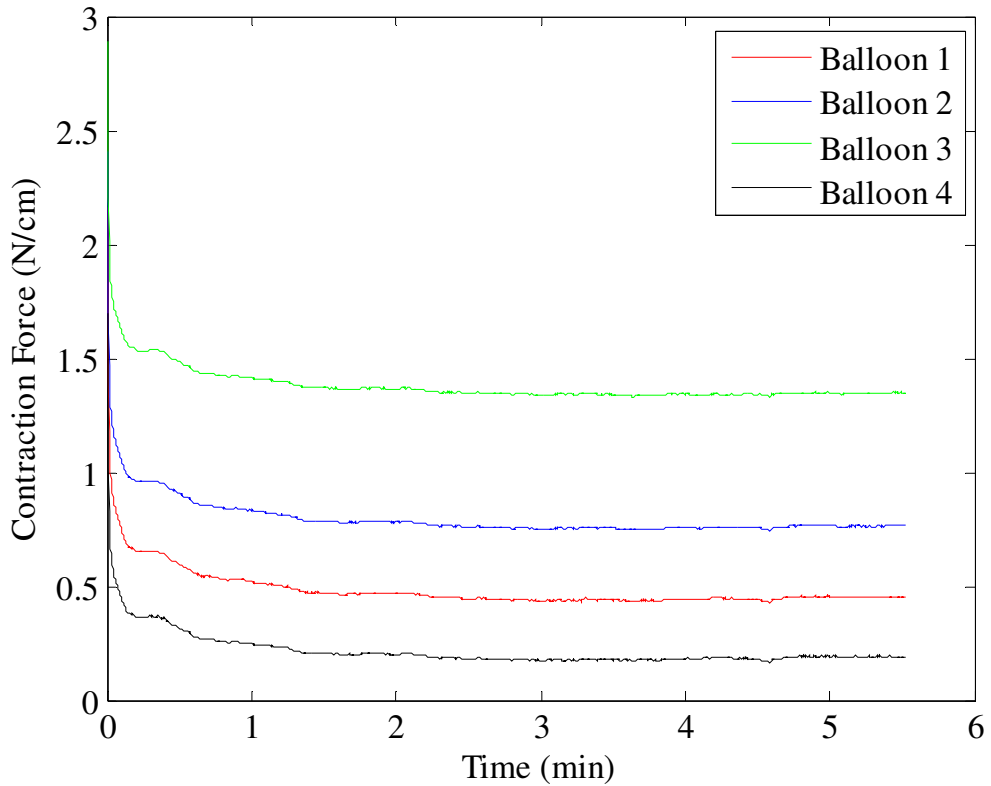


Figure 24: Myenteric contractile response of the human small bowel from a single MFS with four balloon segments.

The visual inspection appears consistent with the results presented in Table 6 with the exception of negative contact force measurements for Balloon 2 and 4 in Studies 1-2 and Balloons 2-4 in Study 4. One possible reason for the negative force readings may be from longitudinal muscle contractions which shorten the small bowel. This could potentially increase the lumen diameter around the MFS and induce a negative force on the balloons. Another possible explanation may be the uncertainty associated with a small contact force measurement. The two major sources of uncertainty with the current MFS system stem from the *in vivo* height compensation and syringe pump compensation ( $c_{syringe}$ ). It is difficult to accurately pinpoint the exact location on the side of the patient's abdomen that corresponds to the *in vivo* level of the MFS. Taking this into account, the average uncertainty for the MFS system is approximately  $\pm 0.65$  N/cm which indicates that some of the forces may be too small for the MFS to measure.

## Chapter 5: Conclusion

Through successive design iterations, the migrating motor complex force sensor (MFS), initially developed by Terry *et al.* has been successfully modified to collect data inside a human in a sterile, minimally invasive fashion. To the author's knowledge, the data presented in this study provide the first known myenteric contact force measurement against a solid bolus in a human small intestine. The results, while in the lower range, are consistent with theoretical models and will serve as an essential design parameter for researchers developing robotic capsule endoscopes [13-14].

An intriguing observation is the effect of anesthesia on contact force. Akkurt *et al.* compared the effects of intravenous (IV) propofol anesthesia versus desflurane gas anesthesia on human GI motility [22]. They found that patients who received the IV anesthesia had their first post-operative bowel movement in less time than those who received the desflurane gas. Future work may focus on the effects of anesthesia on contact force.

Another avenue of future research is to develop a solid-state version of the MFS. Doing so would eliminate the effects of hydrostatic pressure on the MFS which is the most significant source of error in the current system. An additional

benefit of solid-state manometry is that it permits the collection of data in a subject for an extended period of time in an ambulatory setting. Adapting this technology in a future MFS may allow a full MMC cycle to be recorded.

## References

1. U.S. Cancer Statistics Working Group, "United States Cancer Statistics: 1999-2010 Incidence and Mortality Web-based Report," Atlanta (GA): Department of Health and Human Services, Centers for Disease Control and Prevention, and National Cancer Institute, 2013. [Online]. Available: <http://www.cdc.gov/cancer/colorectal/statistics>.
2. A. Moglia, A. Menciassi, M. Schurr, and P. Dario, "Wireless capsule endoscopy: from diagnostic devices to multipurpose robotic systems," *Biomed Microdevices*, vol. 9, pp. 235-243, 2007.
3. M. F. McGee, M. J. Rosen, J. Marks, R. P. Onders, A. Chak, A. Faulx, V. K. Chen, and J. Ponsky, "A Primer on Natural Orifice Transluminal Endoscopic Surgery: Building a New Paradigm," *Surgical Innovation*, vol. 13, no. 2, pp. 86-93, Jun. 2006.
4. B. S. Terry, A. B. Lyle, J. A. Schoen, and M. E. Rentschler, "Preliminary Mechanical Characterization of the Small Bowel for *In Vivo* Robotic Mobility," *J. Biomech. Eng.*, vol. 133, no. 9, pp. 091010-7, 2011.
5. B. S. Terry, J. A. Schoen, and M. E. Rentschler, "Characterization and Experimental Results of a Novel Sensor for Measuring the Contact Force from Myenteric Contractions," *IEEE Transactions on Biomedical Engineering*, vol. 59, no. 7, pp. 1971-1977, 2012.
6. B. S. Terry, J. A. Schoen, and M. E. Rentschler, "Measurements of the contact force from myenteric contractions on a solid bolus," *J. Robotic Surg.*, vol. 7, pp. 53-57, 2013.
7. R. L. Drake, A. W. Vogl, and A. Mitchell, *Gray's Anatomy for Students*. Churchill Livingstone, 2010.
8. G. Glass, *Introduction to Gastrointestinal Physiology*. Prentice-Hall, Inc., 1968.
9. D. U. Silverthorn, *Human Physiology: An Integrated Approach*. Pearson, 2010.
10. H. Gregersen, *Biomechanics of the Gastrointestinal Tract*. Springer, 2003.

11. H. Seidl, F. Gundling, A. Pfeiffer, C. Pehl, W. Schepp, and T. Schmidt, "Comparison of small-bowel motility of the human jejunum and ileum," *Neurogastroenterology and Motility*, vol. 24, pp. 373-380, 2012.
12. A. Bertuzzi, S. Salinari, R. Mancinelli, and M. Pescatori, "Peristaltic transport of a solid bolus," *Journal of Biomechanics*, vol. 16, no. 7, pp. 459-464, 1983.
13. R. Miftahof and E. Fedotov, "Intestinal propulsion of a solid non-deformable bolus," *Journal of Theoretical Biology*, vol. 235, no. 1, pp. 57-70, Jul. 2005.
14. R. Miftahof and N. Akhmadeev, "Dynamics of intestinal propulsion," *Journal of Theoretical Biology*, vol. 246, no. 2, pp. 377-393, May 2007.
15. R. Andrew, "Gastric, duodenal jejunal motility in man; physiological studies by balloon-kymography," *Austral. J. exp. Biol.*, vol. 32, pp. 479-488, 1954.
16. E. Clinton Texter, "Pressure and transit in the small intestine," *Digestive Diseases and Sciences*, vol. 13, no. 5, pp. 443-454, May 1968.
17. R. E. Clouse, and A. Staiano, "Topography of normal and high-amplitude esophageal peristalsis," *Am J Physiol.*, vol. 265, pp. G1098-1107, 1993.
18. R. E. Clouse, A. Staiano, A. Alrakawi, L. Haroian, "Application of topographical methods to clinical esophageal manometry," *Am J Gastroenterol.*, vol. 95, pp.2720-2730, 2000.
19. M. Fox, G. Hebbard, P. Janiak, J. G. Brasseur, S. Ghosh, M. Thumshirn, "High-resolution manometry predicts the success of oesophageal bolus transport and identifies clinically important abnormalities not detected by conventional manometry," *Neurogastroenterol Motil.*, vol. 16, pp. 533-542, 2004.
20. S. K. Sarna, K. H. Soergel, R. P. Ryau, C. M. Wood, R. C. Arndorfer, "Prolonged intubation of the small intestine alters the migrating motor complex in humans," *Gastroenterology*, vol. 102, pp. A509, 1992.
21. O. Liem, R. E. Burgers, F. L. Connor, M. A. Benninga, S. N. Reddy, H. M. Mousa, and C. Di Lorenzo, "Solid-state vs water-perfused catheters to measure colonic high-amplitude propagating contractions," *Neurogastroenterology and Motility*, vol. 24, pp. 345-e167, 2012.
22. B. C. Akkurt, M. Temiz, K. Inanoglu, A. Asian, S. Turhanoglu, Z. Asfuroflu, E. Canbolant, "Comparison of recovery characteristics, postoperative nausea

and vomiting, and gastrointestinal motility with total intravenous anesthesia with propofol versus inhalation anesthesia with desflurane for laparoscopic cholecystectomy: A randomized controlled study." *Current Therapeutic Research*, vol. 70, no. 2, pp. 94-103, April 2009.

# Appendices

## Appendix A: MFS Balloon Fabrication Procedure

1. Slowly dip molds in silicone dispersion (Fig 25) and rotate with motor set to 2V for 3 hours (Fig 26). All steps prior to baking should be done in a fume hood.
2. Slowly dip molds in silicone dispersion again and rotate with motor set to 2V for 6 hours.
3. Stop rotation and let the molds sit overnight.
4. Bake the silicone covered molds in an oven at 150°C for 2.5 hours.
5. After baking is complete, remove from oven and let sit for at least 4 hours.
6. Use a 1/4 in. hole punch to remove the inner radius from both sides of each balloon.
7. Peel balloons from molds.

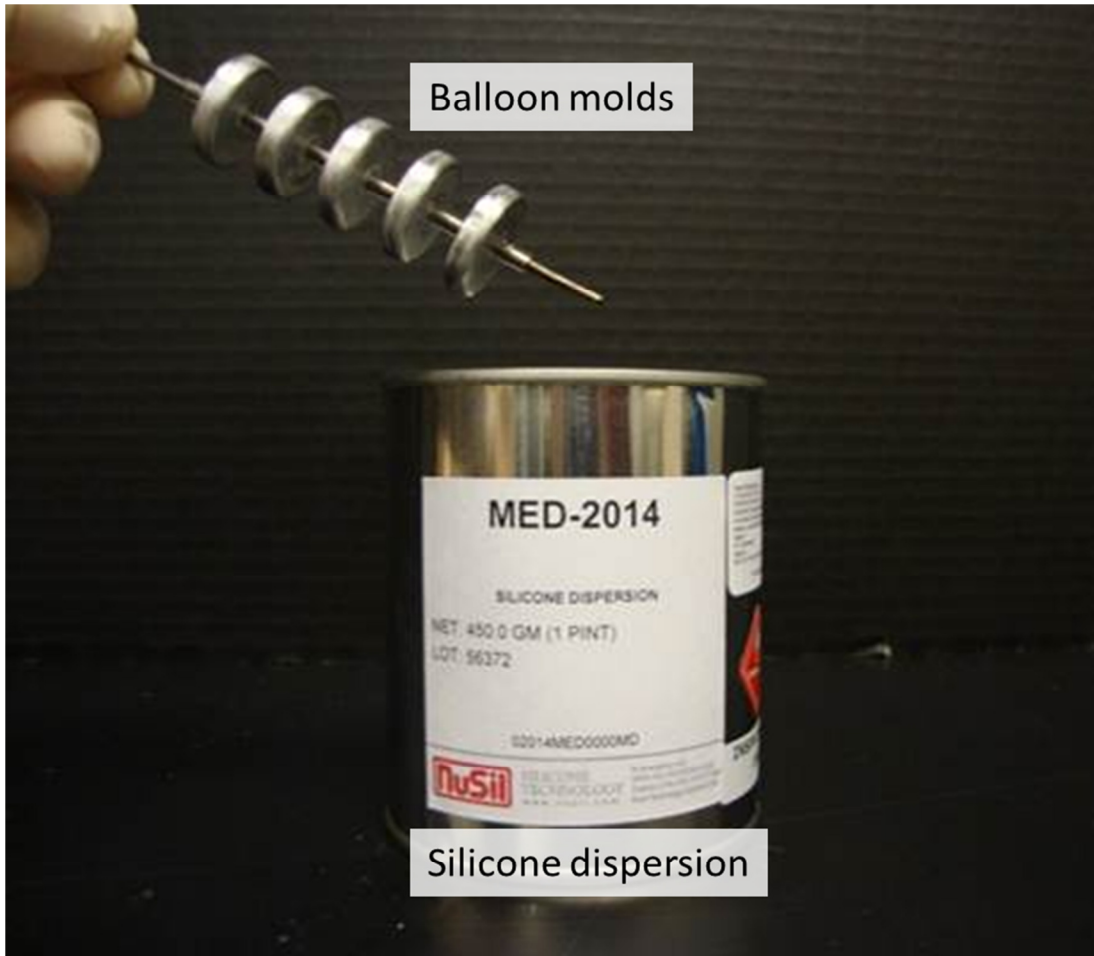


Figure 25: Balloon molds being dipped into silicone dispersion.

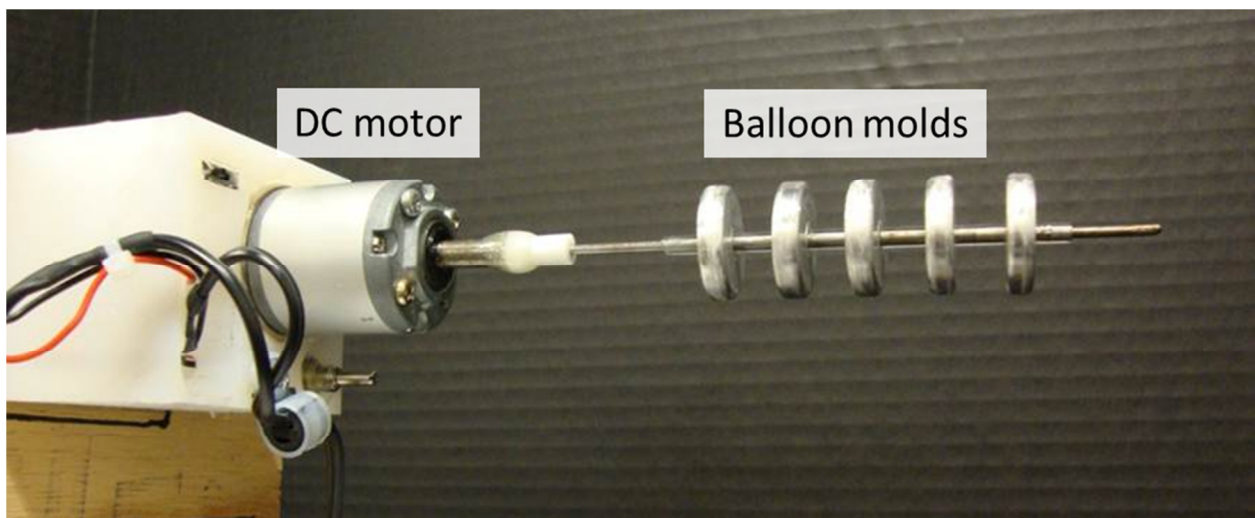


Figure 26: Balloon molds being rotated.

## Appendix B: MFS Gasket Fabrication Procedure

1. Punch four gaskets from a 1/8 in. thick Viton® Rubber sheet using a 3/8 in. hole punch.
2. Use a 1/4 in. hole punch to remove the center from each gasket.
3. Heat a sharp metal object using a soldering iron and pierce it through the gasket to create a small hole (Fig 27).
4. Push the PTFE tube through the balloon hub and gasket (Fig 28).
5. Pull the gasket over the hub (Fig 29).

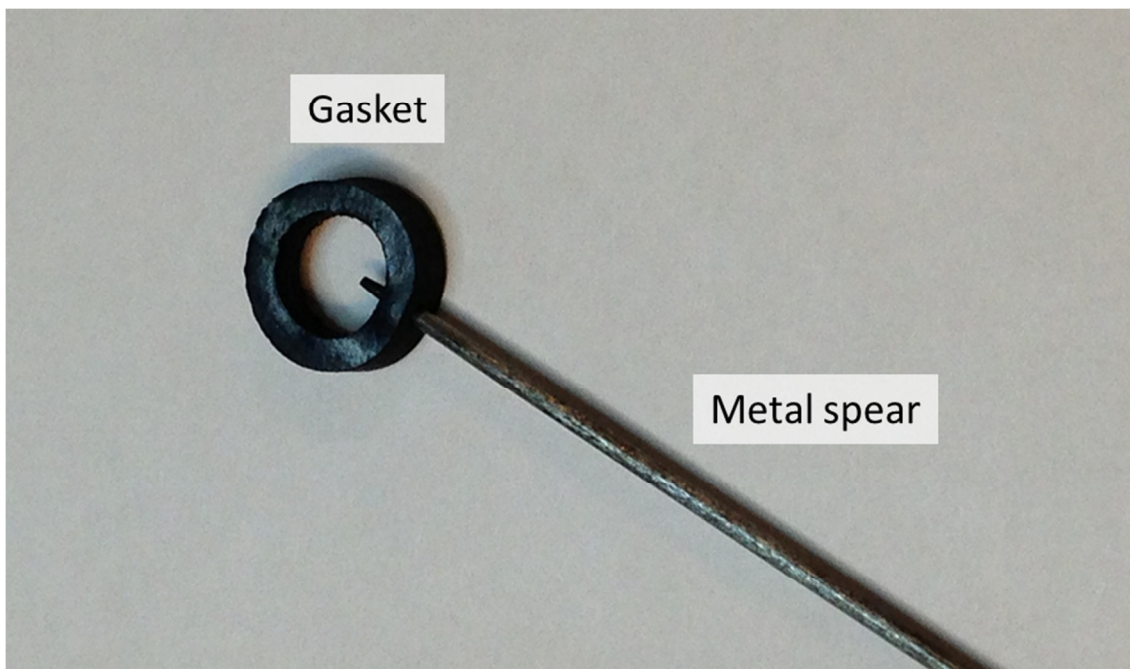


Figure 27: Metal spear piercing the MFS gasket.

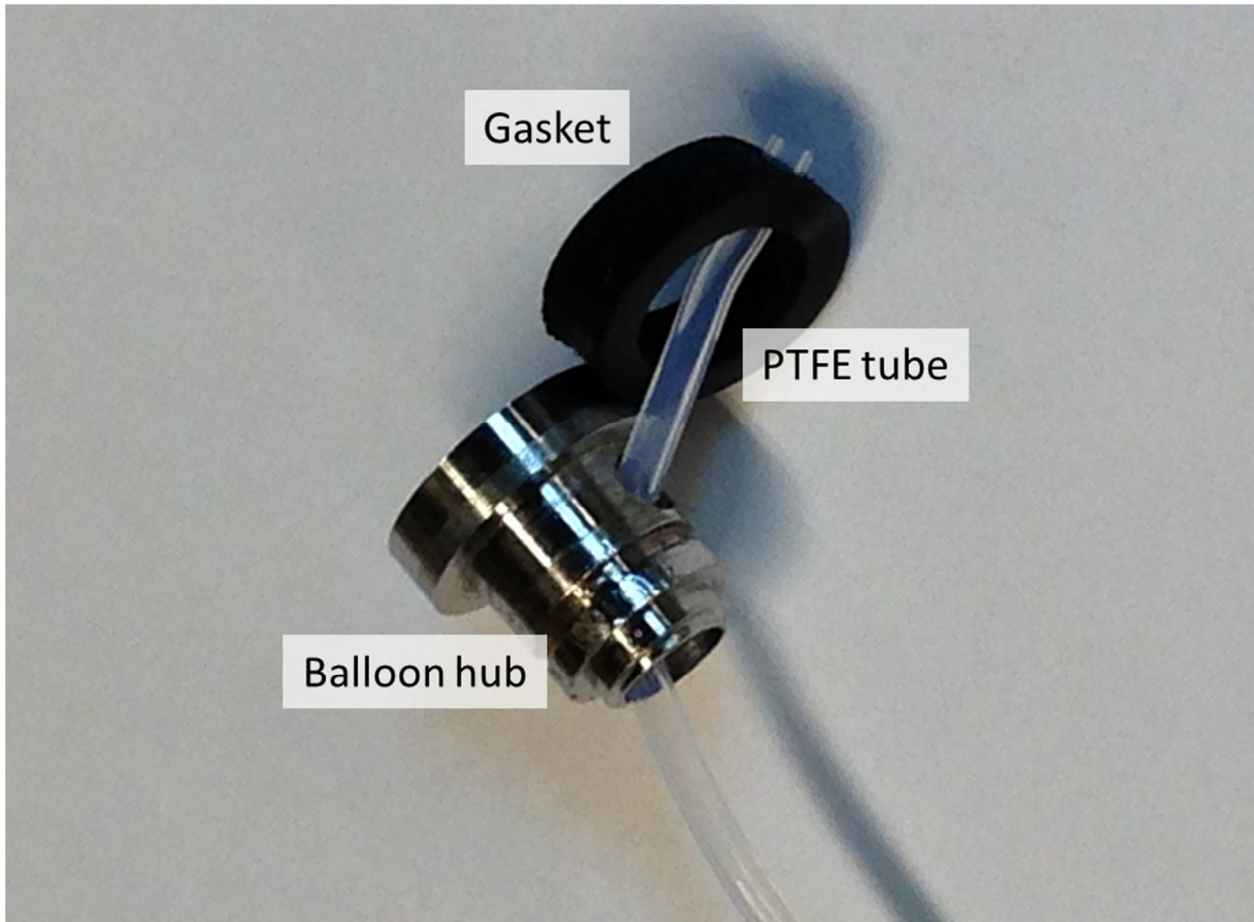


Figure 28: PTFE tube inserted through the hub and gasket.

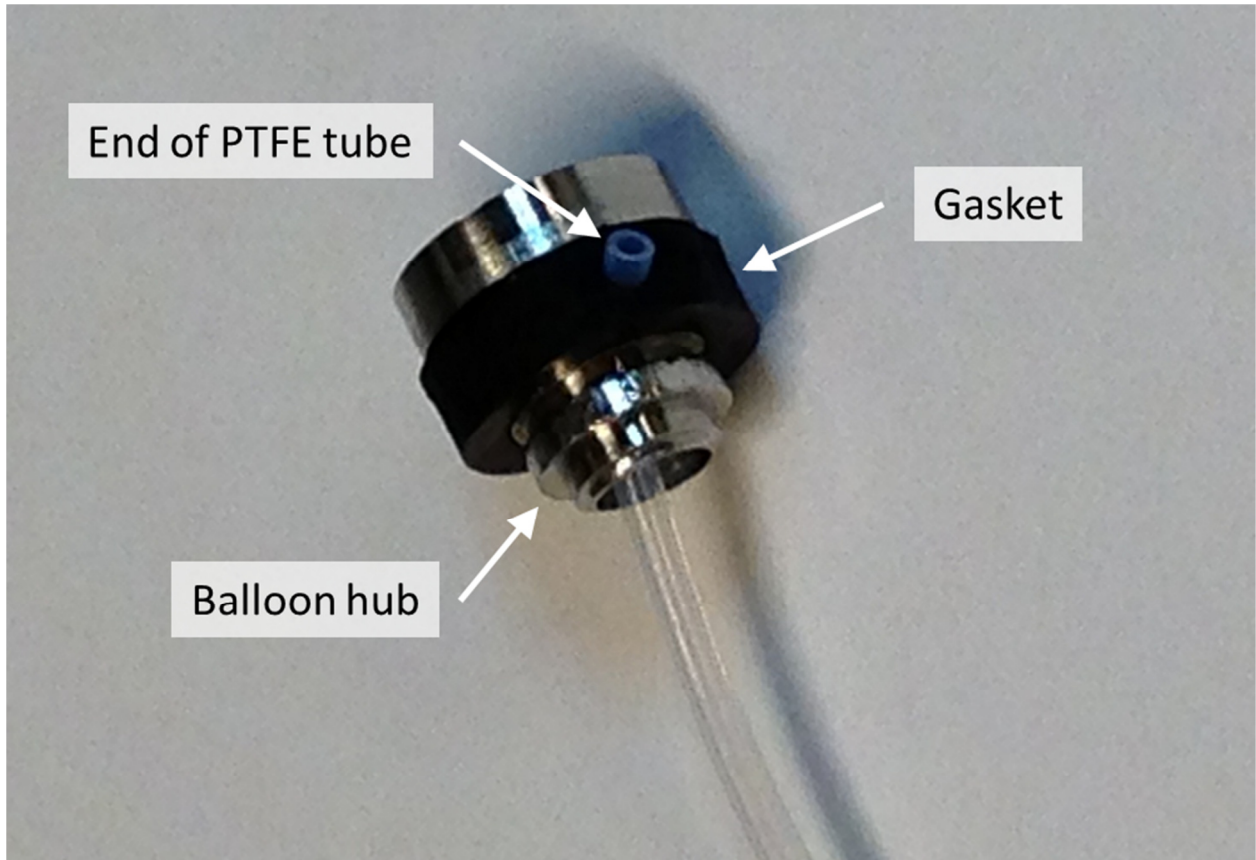


Figure 29: Gasket seated on the hub ready for a balloon to be attached.

# Appendix C: Material Data Sheet for Silicone Dispersion



Creative Partners in a Material World

NuSil Technology  
 1050 Cindy Lane • Carpinteria, CA 93013  
 805/684-8780 • 805/566-9905 Fax  
 www.nusil.com

An ISO 9001 Certified Company

# MED-2014

Silicone Dispersion

## Product Profile

### Description

- Fully compounded, platinum-catalyzed, dimethyl-methylvinyl siloxane elastomers dispersed in xylene
- Heat-cured to form strong, thin, elastomeric films
- Excellent physical properties
- Usable life can be extended with refrigeration

### Applications

- For fabricating variously shaped elastomeric parts by brushing, spraying, or dipping
- Used for making membranes or cast film

**NuSil Technology's MED-2014 is a restricted products. It shall not be considered for use in human implantation for a period of greater than 29 days.**

Typical Properties	Result	Metric Conv.	ASTM	NT-TM
<b>Uncured:</b>				
Appearance	Translucent	-	D2090	002
Viscosity	3,400 cP	3,400 mPas	D445	001
Non-Volatile Content	35%	-	D2288	004
<b>Cured:</b> 60 min. @ 50°C; 60 min. @ 150°C; Stabilize 3 hours minimum @ ambient temperature and humidity				
Specific Gravity	1.10	-	D792	003
Durometer, Type A	35	-	D2240	006
Tensile Strength	1,800 psi	12.4 MPa	D412, D882	007
Elongation	800%	-	D412, D882	007
Tear Strength, die B	185 psi	33.6 k/Nm	D624	009

### Instructions for Use

Thin MED-2014 to the desired consistency with xylene, the suggested solvent. Mix the material thoroughly before use. Achieve best results by filtering the dispersion appropriately before use. Take care to avoid solvent evaporation and air entrapment.

When using any solvent, always provide adequate ventilation and avoid skin contact. Follow manufacturer's label instructions and refer to appropriate MSDS.

The mold, mandrel, or part being coated with dispersion should be free from contamination, not inhibit the cure, and be able to withstand the cure cycle. Apply the dispersion by brushing, spraying, or dipping. Control the thickness by building up successive, thin (1-2 mil) coats. Allow the bulk of the solvent to evaporate between coats. When the desired thickness is obtained, set aside the coated object and allow the solvent to completely evaporate. Controlled low-humidity conditions will reduce bubbles while coating.

### Packaging

- 1 Pint (450 g)
- 1 Gallon (3.6 kg)
- 5 Gallon (18.0 kg)

### Warranty

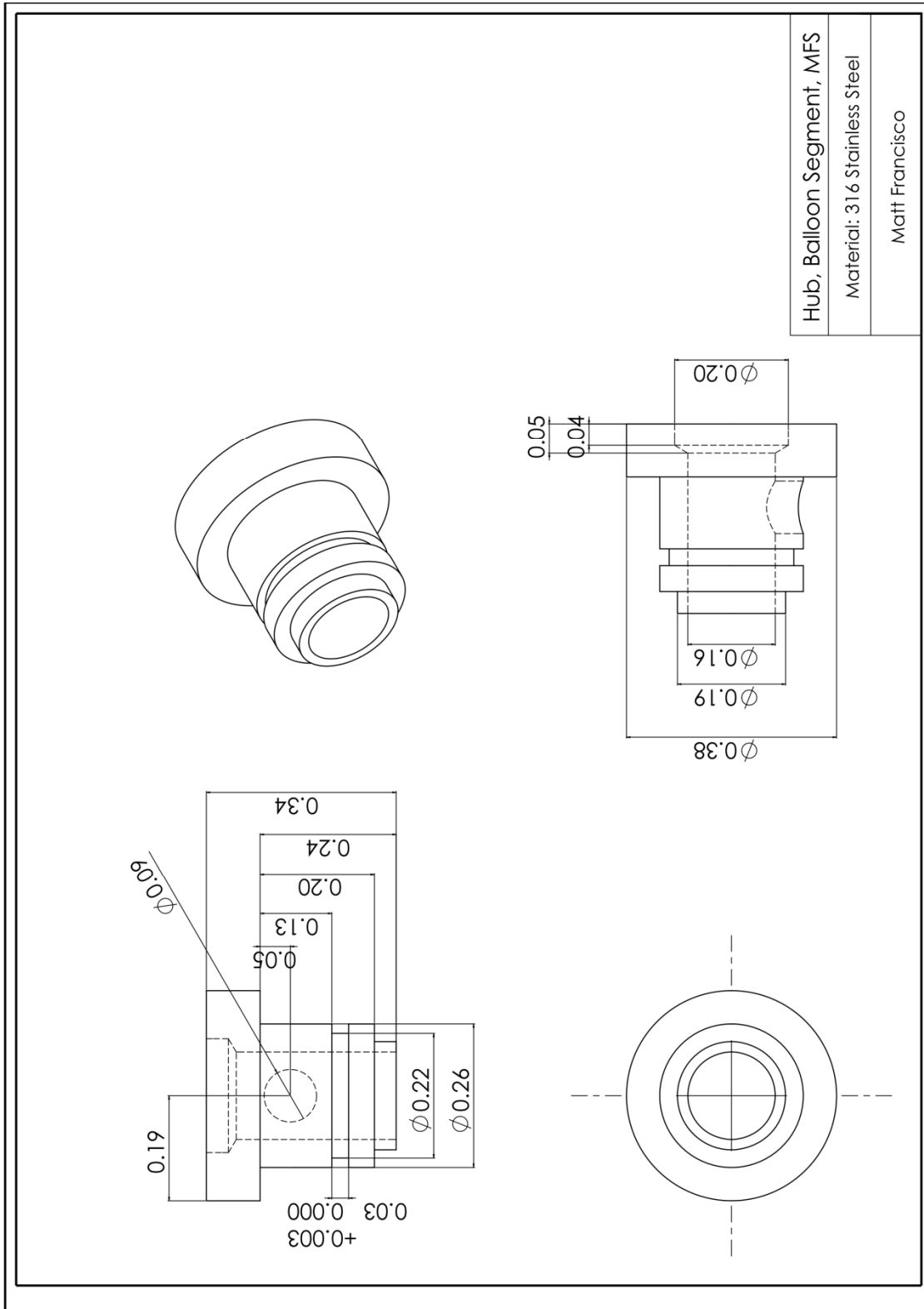
3 Months

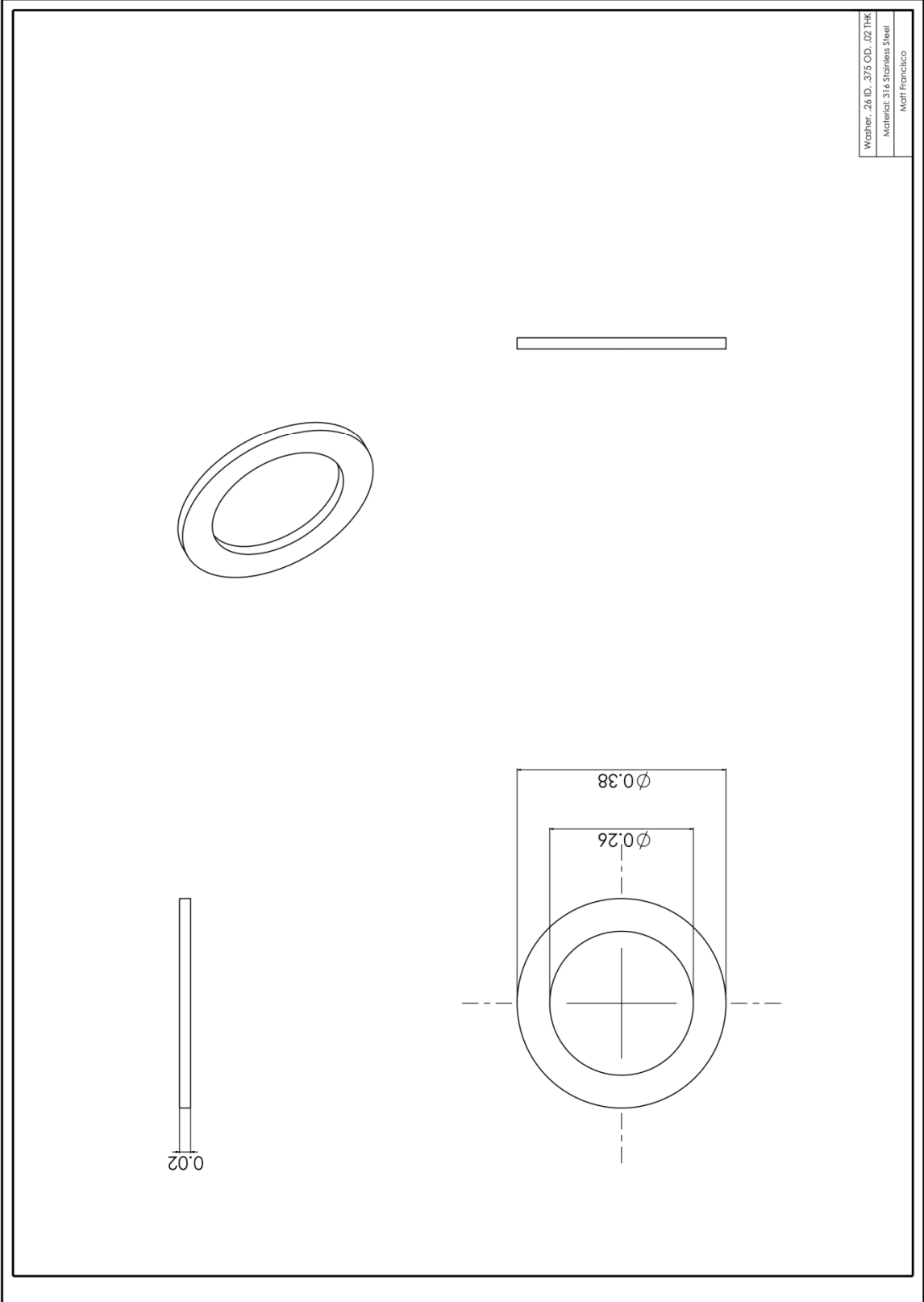
### Caution

MED-2014 will cure in contact with most materials. Exceptions include butyl, latex, chlorinated rubbers, some RTV silicones, and unreacted residues of some curing agents.

MED-2014 27 December 2006

# Appendix D: SolidWorks Part Drawings for MFS Hub Fabrication



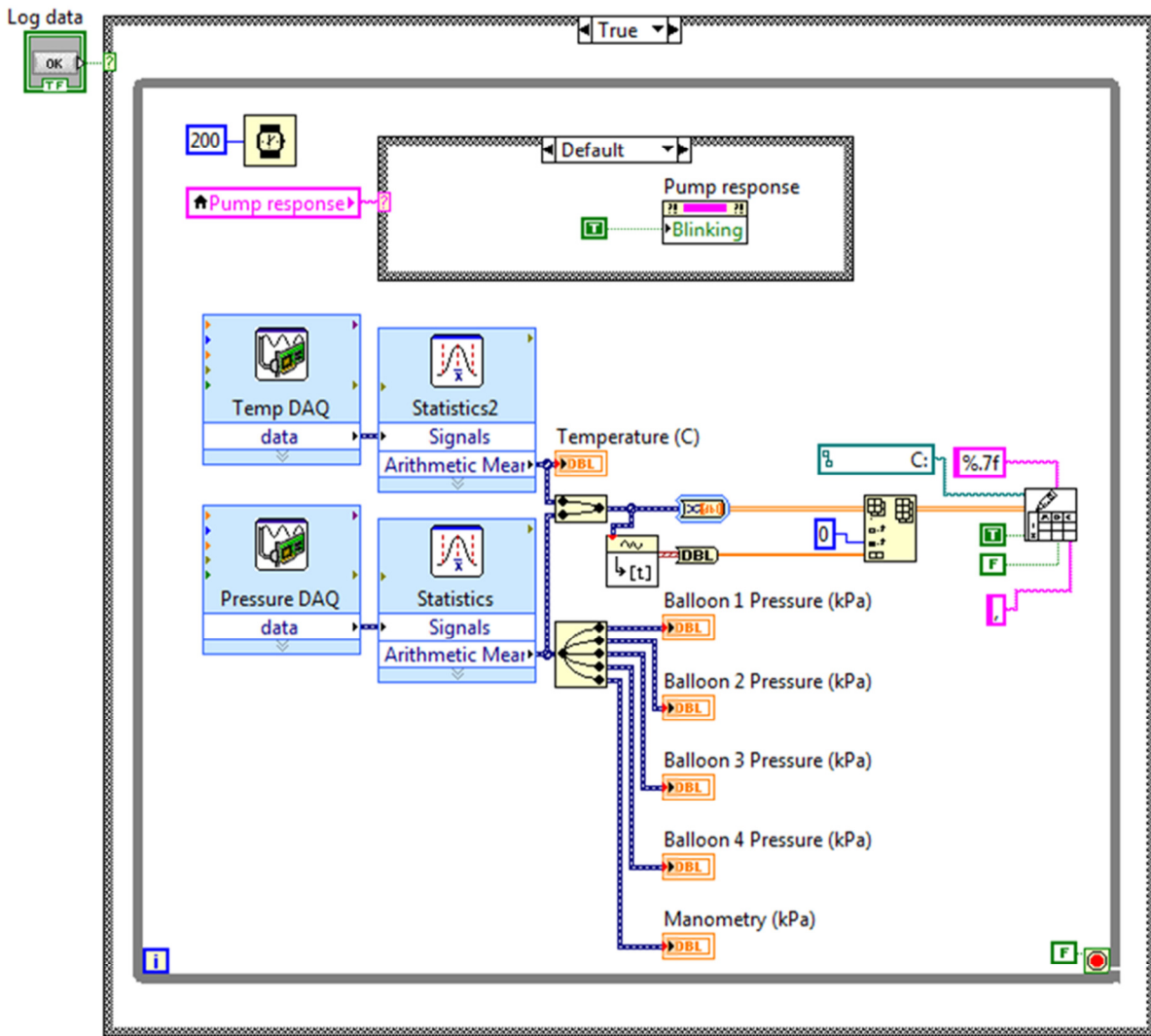


## Appendix E: LabVIEW Code Used to Operate the Syringe Pump

Note: The following code is not exhaustive. The full code is archived on a directory in the Advanced Medical Technologies Laboratory file server at:

\\amd.colorado.edu\terrybs\working\Intestinal Crawler\VIs\MFSPressurize.vi

Access to this file server is limited to members of the Advanced Medical Technologies Laboratory.



## Appendix F: Matlab Code Used for MFS Characterization

The following code is “Main\_ExtractFeatures.m” which extracts certain key features from the raw characterization data.

```
% The purpose of this script is to extract relevant features from the data
% gathered during characterization of the MFS sensor. Features extracted
% from this script are then used by the Main_Fit.m script found in this
% folder.
clearvars;
close all;

% Load the characterization data
files = {'MFSSensorCharVoltagesS2B3.csv', 'MFSSensorCharTempS2B3.csv'};
saveFiles = {'S2B3'};

DECAY_CHAR_REGION = {[18000:18050 170000:170050]};
END_OF_LAST_CYCLE = [153100];

%%
%
for f = 1 : length(saveFiles)
    % Column locations of the characterization data
    MFS_PRESS_COL = 4;
    AMB_TEMP_COL = 2;
    AMB_PRESS_COL = 6;
    FORCE_COL = 12;
    EXTEN_COL = 13;
    TIME_COL = 1;
    globalFitDataInd = 0;

    V = importdata(files{2 * f - 1});
    V = V.data;
    T = importdata(files{2 * f});
    T = T.data;

    % When stopping the signal express program, boards don't stop at the same
    time.
    if length(V) < length(T)
        T = T(1:length(V),:);
    else
        V = V(1:length(T),:);
    end

    D = [V(:, TIME_COL) V(:, MFS_PRESS_COL) V(:, AMB_PRESS_COL) T(:,
    AMB_TEMP_COL) V(:, EXTEN_COL) V(:, FORCE_COL) V(:, FORCE_COL)
    zeros(length(V), 1) zeros(length(V), 1)];
```

```

clear('V', 'T');
MFS_PRESS_COL = 2;
ADJ_MFS_PRESS_COL = 9;
AMB_TEMP_COL = 4;
AMB_PRESS_COL = 3;
FORCE_COL = 6;
ADJ_FORCE_COL = 7;
LOCATION_COL = 8; % Location along the circumference of the balloon.
EXTEN_COL = 5;
TIME_COL = 1;
LOCATIONS = [1 2 3];
%%
% Tare the time, ambient pressure, MFS temperature, MFS pressure
AMB_PRESS_TARE_REGION = 16000:17000;
AMBIENT_TEMP_TARE_REGION = 10000:11000;
MFS_PRESS_TARE_REGION = DECAY_CHAR_REGION{f}(1:20); % This gives us the
front end of the decay char region (51:100 is the back end).

D(:, TIME_COL) = D(:, TIME_COL) - D(1, TIME_COL);
D(:, AMB_PRESS_COL) = D(:, AMB_PRESS_COL) - mean(D(AMB_PRESS_TARE_REGION,
AMB_PRESS_COL));
D(:, AMB_TEMP_COL) = D(:, AMB_TEMP_COL) - mean(D(AMBIENT_TEMP_TARE_REGION,
AMB_TEMP_COL));
D(:, MFS_PRESS_COL) = D(:, MFS_PRESS_COL) - mean(D(MFS_PRESS_TARE_REGION,
MFS_PRESS_COL));
figure; H = plot(D(:, TIME_COL)/60, D(:, [MFS_PRESS_COL AMB_PRESS_COL
FORCE_COL AMB_TEMP_COL]));
set(H(1), 'Color', 'r');
set(H(2), 'Color', 'b');
set(H(3), 'Color', 'm');
set(H(4), 'Color', 'g');
legend({'MFS Pressure (kPa)', 'Ambient Pressure (kPa)', 'Contact Force
(N)', 'MFS Temperature (deg C)'});
title('MFS characterization tared inputs');
xlabel('Time (m)')

%%
% A cycle consists of one pressure, one temperature and contact data with
% three locations along the balloon circumference. A cycle begins with
characterization of
% the friction of the plunger linear bearing. Identify the cycle
% locations in the data so we can work with smaller chunks for plotting
and
% analysis.
UPPER_BOUND = 4;
LOWER_BOUND = 2;
MIN_MAXIMA_DISTANCE = 140;
MAX_PAIR_DISTANCE = 500;
cycleInd = localmaxima2(-D(:, EXTEN_COL), UPPER_BOUND, LOWER_BOUND,
MIN_MAXIMA_DISTANCE); % This finds the two linear bearing characterization
peaks correlating to the start of each cycle.
cycleInd = findPairs(cycleInd, MAX_PAIR_DISTANCE);
cycleInd = cycleInd(1:2:end) - 300; % Put the index markers prior to the
start of each cycle.

```

```

figure;
%plot(cycleInd, D(cycleInd,EXTEN_COL), 'r*'); hold on;
%plot(D(:,EXTEN_COL), 'b');

cInd = cell(length(cycleInd), 1);

for i = 1 : length(cycleInd)
    if i == length(cycleInd)
        cInd{i} = cycleInd(i):END_OF_LAST_CYCLE(f);
    else
        cInd{i} = cycleInd(i):cycleInd(i + 1);
    end

    %figure;
    %plot(D(cInd{i},TIME_COL), D(cInd{i},2:7), '.', 'MarkerSize', 6)
    %legend('MFS Press', 'Ambient Press', 'MFS Temp', 'Ambient Temp',
'Ext', 'Force');
end

%%
% Remove effects from the pressure decay due to elastomeric creep
DETREND_REGION = DECAY_CHAR_REGION{f}(1):DECAY_CHAR_REGION{f}(end);
decay = DecayCurveLinear(D(DECAY_CHAR_REGION{f}, [TIME_COL
MFS_PRESS_COL]), D(DETREND_REGION, TIME_COL));
%figure; hold on;
%plot(D(DECAY_CHAR_REGION{f}, [TIME_COL]),
D(DECAY_CHAR_REGION{f}, [MFS_PRESS_COL]), 'b.')
%plot(D(DETREND_REGION, [TIME_COL]), decay + D(DECAY_CHAR_REGION{f}(1),
MFS_PRESS_COL), 'r.', 'MarkerSize', 1)
D(DETREND_REGION, ADJ_MFS_PRESS_COL) = D(DETREND_REGION, MFS_PRESS_COL) -
decay;
%figure; hold on;
%plot(D(DETREND_REGION, MFS_PRESS_COL), 'b.')
%plot(D(DETREND_REGION, ADJ_MFS_PRESS_COL), 'r.', 'MarkerSize', 1);

for c = 1:length(cInd)

    fitDataInd = 0;
    %figure; hold on;
    %plot(D(cInd{c},TIME_COL), D(cInd{c},2:6), '.', 'MarkerSize', 6)
    %legend('MFS Press', 'Ambient Press', 'Ambient Temp', 'Ext',
'Force');

    %%
    % Characterize the friction effects, and remove them from the force
data.

    % We need to capture all the peaks of the extension data. The
    % first 2 peaks are used for finding the average friction force
    % from the plunger moving up and down.
    UPPER_BOUND = 5.5;
    LOWER_BOUND = 2.2;

    % Locate change in extension direction
    peakInd = localmaxima2(abs(D(cInd{c}, EXTEN_COL)), UPPER_BOUND,
LOWER_BOUND, MIN_MAXIMA_DISTANCE);

```

```

        dirChangeInd = locateContactCycles(abs(D(cInd{c}, EXTEN_COL)),
peakInd, .015);
        plot(D(cInd{c}(dirChangeInd), TIME_COL),
D(cInd{c}(dirChangeInd), EXTEN_COL), 'r*')
        plot(D(cInd{c}(1:end -1), TIME_COL), abs(diff(D(cInd{c},
FORCE_COL))))

        % Find the average friction force for the plunger moving up and down
        % that occurs when there is no other load on the plunger.
        % Remove 5 points from each each to eliminate the non-steady-state
regions.
        ffUp = mean(D(cInd{c}(dirChangeInd(2) + 5:dirChangeInd(3) - 5),
FORCE_COL));
        ffDown = mean(D(cInd{c}(dirChangeInd(4) + 5:dirChangeInd(5) - 5),
FORCE_COL));

        % Subtract average friction force based on direction of the plunger.
        speed = diff(D(cInd{c}, EXTEN_COL));
        HALF_EXTENSION_SPEED = 0.01;
        D(cInd{c}(speed > HALF_EXTENSION_SPEED), ADJ_FORCE_COL) =
(D(cInd{c}(speed > HALF_EXTENSION_SPEED), FORCE_COL) - ffUp) * 2; % Multiply
by two to include the reaction force at the hub where the device is held
during the test.
        D(cInd{c}(speed < -HALF_EXTENSION_SPEED), ADJ_FORCE_COL) =
(D(cInd{c}(speed < -HALF_EXTENSION_SPEED), FORCE_COL) - ffDown) * 2; %
Multiply by two to include the reaction force at the hub where the device is
held during the test.
        %figure; plot(D(cInd{c}, FORCE_COL), 'r.');
```

hold on;

```

        %plot(D(cInd{c}, ADJ_FORCE_COL), 'b.');
```

%%

```

        % Locate the regions in this cycle that will be used for fitting the
        % characterization equation. We will use regions of active
compression
        % except in the vicinity of a change in the plunger's direction (the
        % complex friction that occurs in this region was not characterized).
Also,
        % identify the LOCATION_X regions.

        % Identify the LOCATION_X regions corresponding to the different
points
        % along the circumference of the MFS that were contacted.
for i = 1:length(LOCATIONS)
        D(cInd{c}(dirChangeInd(9 * i - 2):dirChangeInd(9 * i + 6)),
LOCATION_COL) = LOCATIONS(i);
end

        % The data at the contact peak maxima is unreliable because of the
        % transient friction effects of the linear bearing when the plunger
changes
        % direction (hence we subtract 5 data points, 4 on the left, 1 on the
right).
        % Use data from either side of the maxima, down to the troughs
        % on either side. We also remove the pre-engagement points on either
end
        % before the plunger contacts the sensor.
```

```

    PRE_ENGAGEMENT_REGION = 50; % These are the points to EXCLUDE on
either side of the peak points.

    PEAKS = [8 11 14 17 20 23 26 29 32];
    for i = 1:length(PEAKS)
        fitDataInd = [fitDataInd; ...
            (dirChangeInd(PEAKS(i) - 1) + PRE_ENGAGEMENT_REGION :
dirChangeInd(PEAKS(i)) - 4)']; ...
            (dirChangeInd(PEAKS(i)) + 1 : dirChangeInd(PEAKS(i) + 1) -
PRE_ENGAGEMENT_REGION)'];
        end

        fitDataInd = fitDataInd(2:end);

        globalFitDataInd = [globalFitDataInd; (cInd{c}(fitDataInd(2:end)))'];

        if (c == 1)
            globalFitDataInd = globalFitDataInd(2:end);
        end

        %figure;
        %plot(D(cInd{c}(fitDataInd), TIME_COL), D(cInd{c}(fitDataInd),
[ADJ_MFS_PRESS_COL AMB_TEMP_COL AMB_PRESS_COL ADJ_FORCE_COL LOCATION_COL]),
'.');
        %legend({'ADJ_MFS_PRESS_COL', 'AMB_TEMP_COL', 'AMB_PRESS_COL',
'ADJ_FORCE_COL', 'LOCATION_COL'});
        end

    %%
    % Plot and save data that will be used for fitting

    H = plot(D(globalFitDataInd, TIME_COL)/60, D(globalFitDataInd,
[ADJ_MFS_PRESS_COL AMB_PRESS_COL ADJ_FORCE_COL AMB_TEMP_COL LOCATION_COL]),
'.');
    set(H(1), 'Color', 'r');
    set(H(2), 'Color', 'b');
    set(H(3), 'Color', 'm');
    set(H(4), 'Color', 'g');
    set(H(5), 'Color', 'k');

    legend({'MFS Pressure (kPa)', 'Ambient Pressure (kPa)', 'Contact Force
(N)', 'MFS Temperature (deg C)', 'Location (1..3)'});
    fitData = D(globalFitDataInd, [TIME_COL ADJ_MFS_PRESS_COL AMB_TEMP_COL
AMB_PRESS_COL ADJ_FORCE_COL LOCATION_COL]);
    save([saveFiles{f} '_ExtractedFeatures.mat'], 'fitData');
    xlabel('Time (m)');
    title('MFS characterization, adjusted inputs');
    %%
    %
    TIME_COL = 1;
    ADJ_MFS_PRESS_COL = 2;
    AMB_TEMP_COL = 3;
    AMB_PRESS_COL = 4;
    ADJ_FORCE_COL = 5;
    LOCATION_COL = 6;

```

```

    save([saveFiles{f} '_ExtractedFeaturesCol.mat'], 'TIME_COL',
'ADJ_MFS_PRESS_COL', 'AMB_TEMP_COL', 'AMB_PRESS_COL', 'ADJ_FORCE_COL',
'LOCATION_COL');
    close all;
end

```

The following code is “Main\_Fit.m” which fits the MFS characterization model to the extracted features from “Main\_ExtractFeatures.m”.

```

% Fit the MFS char function to the extracted features data.
clearvars;
close all;
SENSORS = {'S2B3'};
FIT_EQ = 'x(1)*Lc.^2 + x(2)*Lc + x(3)*Pi + x(4)*Pa + x(5)*Ti';
X = zeros(length(SENSORS), 5);
Rsquare_fit = zeros(length(SENSORS),1);
Rsquare_validate = zeros(length(SENSORS),1);
x0 = [0 0 0 0 0];

for i = 1:length(SENSORS)
    load([SENSORS{i} '_ExtractedFeatures.mat']);
    load([SENSORS{i} '_ExtractedFeaturesCol.mat']);

    len = length(fitData);
    ind = 1:floor(len/20):len;
    fitSet = ind(1):ind(2);
    validateSet = ind(2):ind(3);

    for j = 3:2:length(ind) - 2
        fitSet = [fitSet ind(j):ind(j+1)];
        validateSet = [validateSet ind(j+1):ind(j+2)];
    end

    fitSet = [fitSet ind(j+1):ind(j+2)];

    figure(i); hold on;
    plot(fitData(:, ADJ_FORCE_COL), 'b.', 'MarkerSize', 10);
    [x,resnorm,residual,exitflag] = lsqcurvefit(@MFS_char_func, x0, ...
        fitData(fitSet, [LOCATION_COL ADJ_MFS_PRESS_COL AMB_PRESS_COL
AMB_TEMP_COL]), ...
        fitData(fitSet, ADJ_FORCE_COL));

    figure(i);
    plot(fitSet, MFS_char_func(x, fitData(fitSet, [LOCATION_COL
ADJ_MFS_PRESS_COL AMB_PRESS_COL AMB_TEMP_COL])), 'g.', 'MarkerSize', 7);

```

```

    plot(validateSet, MFS_char_func(x, fitData(validateSet, [LOCATION_COL
ADJ_MFS_PRESS_COL AMB_PRESS_COL AMB_TEMP_COL])), 'r.', 'MarkerSize', 7);
    legend('Force response', 'Fitted model', 'Validation');
    ylabel('Force (N)');
    title ('Contact force vs model (fitted and validation)')
    %%
    % Calculate the R^2 values
    Rsquare_fit(i) = 1 - resnorm / norm(fitData(fitSet, ADJ_FORCE_COL) -
mean(fitData(fitSet, ADJ_FORCE_COL)))^2;
    Rsquare_validate(i) = 1 - resnorm / norm(fitData(validateSet,
ADJ_FORCE_COL) - mean(fitData(validateSet, ADJ_FORCE_COL)))^2;

    X(i, :) = x;
end

%%
% Save fit parameters
save('Fit.mat', 'X', 'FIT_EQ', 'Rsquare_fit', 'Rsquare_validate');

```

The following are Matlab function files used within “Main\_Fit.m” and “Main\_ExtractFeatures.m”.

### 1. File name: findPairs.m

```

function pairs = findPairs(vector, maxPairDistance)
    j = 1;

    for i = 1 : length(vector)
        if i < length(vector)
            if (vector(i + 1) - vector(i)) < maxPairDistance
                pairs(j) = vector(i); j = j + 1;
            elseif i > 1
                if (vector(i) - vector(i - 1)) < maxPairDistance
                    pairs(j) = vector(i); j = j + 1;
                end
            end
        elseif i > 1
            if (vector(i) - vector(i - 1)) < maxPairDistance
                pairs(j) = vector(i); j = j + 1;
            end
        end
    end
end

```

## 2. File name: locateContactCycles.m

```
function contactCycleInd = locateContactCycles(vector, peakInd, slope)

    % Identify the foothills of each peak by traversing down one side and
    then
    % stopping when the slope is less than slope, then repeating for the
    % other side. Perform this routine for each peak.

    contactCycleInd = zeros(length(peakInd) * 2, 1);
    j = 1;
    SLOPE_SPAN = 10;

    for i = 1:length(peakInd)

        m = 1;

        while 1
            % Traverse to the left first.
            if (abs(vector(peakInd(i) - m) - vector(peakInd(i) - m -
SLOPE_SPAN)) / SLOPE_SPAN) < slope
                contactCycleInd(j) = peakInd(i) - m; j = j + 1;
                break;
            end

            m = m + 1;
        end

        m = 1;

        while 1
            % Traverse to the right next.
            if (abs(vector(peakInd(i) + m) - vector(peakInd(i) + m +
SLOPE_SPAN)) / SLOPE_SPAN) < slope
                contactCycleInd(j) = peakInd(i) + m; j = j + 1;
                break;
            end

            m = m + 1;
        end
    end

    contactCycleInd = [peakInd'; contactCycleInd];
    contactCycleInd = sort(contactCycleInd);
end
```

### 3. File name: MFS\_calc\_func.m

```
% Contact force (Fc) as a function of:
% Contact location (Lc)
% MFS internal pressure (Pi)
% Ambient pressure (Pa)
% MFS internal temperature (Ti)
% Unknown constants: x
% fitData should be a matrix where the columns are Lc, Pi, Pa, Ti
% See AMD lab book 2 page 63 for a derivation of this equation.

function contactForce = MFS_calc_func(x, fitData)
    Pi = fitData(:,2);
    Pa = fitData(:,3);
    Ti = fitData(:,4);

    Fc = x(1)*14 / 3 + x(2)*2 + x(3)*Pi + x(4)*Pa + x(5)*Ti;

    %plot(Fc, 'r.', 'MarkerSize', 1);
    %drawnow;
    contactForce = Fc;
end
```

### 4. File name: MFS\_char\_func.m

```
% Contact force (Fc) as a function of:
% Contact location (Lc)
% MFS internal pressure (Pi)
% Ambient pressure (Pa)
% MFS internal temperature (Ti)
% Unknown constants: x
% fitData should be a matrix where the columns are Lc, Pi, Pa, Ti
% See AMD lab book 2 page 63 for a derivation of this equation.

function contactForce = MFS_char_func(x, fitData)
    Lc = fitData(:,1);
    Pi = fitData(:,2);
    Pa = fitData(:,3);
    Ti = fitData(:,4);

    Fc = x(1)*Lc.^2 + x(2)*Lc + x(3)*Pi + x(4)*Pa + x(5)*Ti;

    %plot(Fc, 'r.', 'MarkerSize', 1);
    %drawnow;
    contactForce = Fc;
end
```